Top Curr Chem (2014)
DOI: 10.1007/128_2013_460

Quasiparticle Self-Consistent *GW* Method for the Spectral Properties of Complex Materials

Fabien Bruneval and Matteo Gatti

Abstract The *GW* approximation to the formally exact many-body perturbation theory has been applied successfully to materials for several decades. Since the practical calculations are extremely cumbersome, the *GW* self-energy is most commonly evaluated using a first-order perturbative approach: This is the so-called G_0W_0 scheme. However, the G_0W_0 approximation depends heavily on the mean-field theory that is employed as a basis for the perturbation theory. Recently, a procedure to reach a kind of self-consistency within the *GW* framework has been proposed. The quasiparticle self-consistent *GW* (QS*GW*) approximation retains some positive aspects of a self-consistent approach, but circumvents the intricacies of the complete *GW* theory, which is inconveniently based on a non-Hermitian and dynamical self-energy. This new scheme allows one to surmount most of the flaws of the usual G_0W_0 at a moderate calculation cost and at a reasonable implementation burden. In particular, the issues of small band gap semiconductors, of large band gap insulators, and of some transition metal oxides are then cured. The QS*GW* method broadens the range of materials for which the spectral properties can be predicted with confidence.

Keywords Electronic structure · Ab initio calculations · Many-body perturbation theory · GW approximation

F. Bruneval
CEA, DEN, Service de Recherches de Métallurgie Physique, 91191, Gif-sur-Yvette, France
e-mail: fabien.bruneval@cea.fr

M. Gatti (✉)
Laboratoire des Solides Irradiés, École Polytechnique, CNRS-CEA/DSM, 91128, Palaiseau, France

European Theoretical Spectroscopy Facility (ETSF)

Synchrotron SOLEIL, L'Orme des Merisiers, Saint-Aubin, BP 48, 91192, Gif-sur-Yvette, France
e-mail: matteo.gatti@polytechnique.edu

Contents

1 Photoemission Spectroscopy and Methods for Electronic Structure Calculations

Photoemission (PES) is one of the most powerful spectroscopy tools that probe the electronic properties of materials [1, 2]. Direct photoemission is a photon-in electron-out technique: the energy of an incoming photon is used to extract an electron (that is called the photoelectron) from the sample. If N is the initial number of electrons, the electronic system after the electron removal is left in an $(N-1)$-electron state, which can be the ground state or an excited state. By measuring the kinetic energy of the photoelectron, one obtains the ionization energies of the electrons in the system (i.e., the energy required to remove an electron, or, equivalently, to create a hole). The affinity energies (i.e., the energy gained to add an electron to the system) can be analogously obtained by means of inverse photoemission, which is an electron-in photon-out technique. Electron addition and removal energies together define the electronic structure of a material (e.g., its band gap). In particular, when the momentum (and possibly the spin) of the photoelectron is also measured, as in angular-resolved photoemission (ARPES), one gets access to the band structure of the material.

From the theoretical point of view, an accurate description of photoemission spectra is still a great challenge today [3–8]. In the sudden approximation one

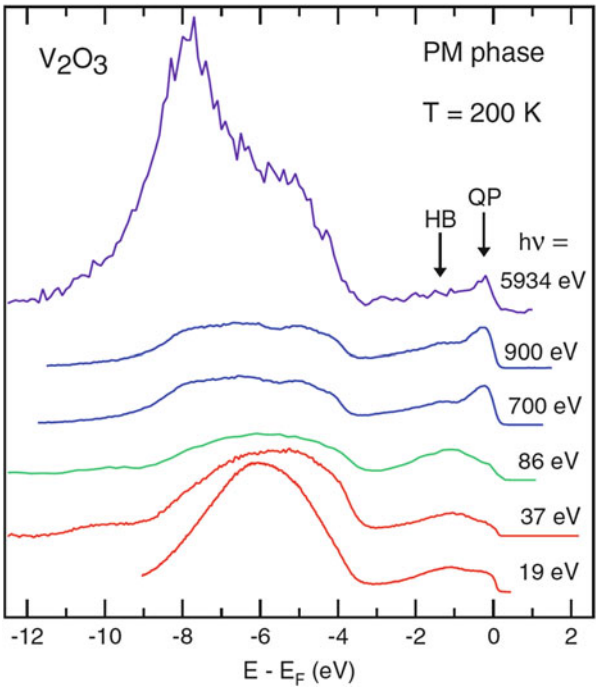

Fig. 1 Experimental photoemission spectra for the valence band of the metallic phase of V_2O_3 for a broad range of photon energies from $h\nu = 19$ eV to $h\nu = 6$ KeV. We observe a strong variation of the spectra with the photon energy. From [9]. Copyright 2009, The American Physical Society

assumes that the photoelectron is immediately decoupled from the sample. In this approximation the measured photocurrent $J_{\mathbf{k}}(\omega)$, which is the probability per unit time of emitting an electron with momentum $\mathbf{k}$ and kinetic energy $E_{\mathbf{k}}$ when the sample is irradiated with photons of frequency ω, is given by [5]

$$J_{\mathbf{k}}(\omega) = \sum_i |\Delta_{\mathbf{k}i}|^2 A_{ii}(E_{\mathbf{k}} - \omega), \tag{1}$$

where we have introduced the matrix elements of the spectral function $A(\omega)$ (for $\omega < \mu$, where μ is the Fermi energy), which are weighted by the photoemission matrix elements $\Delta_{\mathbf{k}i}$ that describe the coupling with the photons. Here we have also assumed that there exists a one-particle basis in which A, rigorously defined as the imaginary part of the one-particle Green's function G (see Sect. 2), is diagonal. While the spectral function A_{ii} is an (intrinsic) property of the (bulk) material, independent of the photon field, photoemission spectra often display an important dependence on the photon properties (see Fig. 1). However, when comparing theoretical results with experimental spectra, most often the photoemission matrix elements are completely neglected, together with the photon-energy dependence of the spectra. Going through the series of drastic assumptions that we have made so far, we see that bridging the gap between theory and experiment is still an important issue.

In the following we will confine our discussion to the electronic properties contained in the spectral function A. In an independent-particle picture the spectral function for occupied states is simply $A_{ii}(\omega) = \delta(\omega - \varepsilon_i)\theta(\mu - \omega)$ and the photocurrent

$$J_{\mathbf{k}}(\omega) = \sum_{i}^{\text{occ}} \delta(E_{\mathbf{k}} - \omega - \varepsilon_i) \tag{2}$$

is hence described by the density of occupied states evaluated at the energy $E_{\mathbf{k}} - \omega$, and is given by a series of delta peaks corresponding to the energies ε_i of the one-particle Hamiltonian. By measuring the kinetic energy of the photoelectron, in an independent-particle picture one would obtain directly the energy of the one-particle level that the electron was occupying before being extracted from the sample. More realistically, as a consequence of the electronic interactions, the delta peaks in the spectral function acquire a finite width, which corresponds to the finite lifetime of the excitation in the electronic system. Generally a broadened peak is still prominent in the spectrum, having a weight Z (called the renormalization factor) as large as 0.6–0.7 (a delta peak has $Z = 1$). In these situations one associates the peak with a quasiparticle (QP) excitation. The collection of the energy positions of the quasiparticle peaks defines the band structure of the material, which is most often the target of the calculations.

However, beyond a quasiparticle picture, the spectral function is generally much richer. In fact, features with lower intensities (the satellites or side bands) are often visible in the spectra. They correspond to situations in which the electronic system is left in an $(N - 1)$-electron excited state which cannot be described by a quasi-hole. Indeed, together with the electron removal, additional excitations (e.g., plasmons) can also be induced in the system by the absorption of the photon. Clearly a calculation of quasiparticle energies only is unable to describe satellites, including Hubbard side bands, which are, by definition, a signature of many-body effects beyond a band-structure description.

Density-functional theory (DFT) [10] is a ground-state theory and hence is not appropriate to describe excitation energies measured in photoemission. In the Kohn–Sham scheme [11] the ground-state density and the ground-state total energy are obtained from a set of fictitious noninteracting electrons. Unfortunately, the eigenvalues ε_i of the Kohn–Sham equation

$$\left(-\frac{\nabla^2}{2} + V_{\text{ext}}(\mathbf{r}) + V_{\text{H}}(\mathbf{r}) + V_{\text{xc}}(\mathbf{r})\right)\phi_i(\mathbf{r}) = \varepsilon_i\phi_i(\mathbf{r}), \tag{3}$$

where V_{ext}, V_{H}, and V_{xc} are respectively the external, Hartree, and exchange-correlation potentials, cannot be interpreted as the additional or removal energies measured in photoemission [12] (except for the HOMO level [13]). In practical applications, the Kohn–Sham band gaps are most commonly smaller than the experimental values. The exact quasiparticle band gap is defined as

$[E(N+1) - E(N)] - [E(N) - E(N-1)]$, where $E(M)$ is the ground-state total energy of M electrons. In finite systems in the "self-consistent field" (Δ-SCF) scheme, these total energies for N, $N \pm 1$ electrons can be calculated explicitly and approximations to V_{xc} can give good results for the band gaps, since they can describe Hartree relaxation effects well [14]. The variation of the electron density $\delta\rho$ for adding or removing an electron scales as $1/N$: thus in an infinite system $\delta\rho \to 0$. In this limit the Δ-SCF scheme yields, with analytic functionals of the density such the local-density approximation (LDA) [11], the Kohn–Sham band gap [15]. In exact Kohn–Sham theory a nonanalytic, discontinuous change in V_{xc} with respect to change in the electron number must be present [16–18].

Even in the homogeneous electron gas, where the local-density approximation is exact for the total energies by definition, the discontinuity of the momentum distribution at the Fermi surface (which corresponds to the renormalization factor Z) and spectral properties such as lifetimes and satellites remain inaccessible in the Kohn–Sham formalism [19, 20]. The momentum distribution, for instance, can be accurately calculated using Quantum Monte Carlo (QMC) techniques [19], but excitations contained in the spectral function cannot be easily calculated in QMC at the moment. Accurate quantum chemical methods, such as full configuration interaction or coupled-cluster techniques, have been developed for molecular systems, but until recently they have not been explored in solids for their high computational complexity [21].

In spectroscopy one is often interested in specific answers to limited questions and there is no need to calculate the full many-body wavefunction, which contains more information than necessary. A successful strategy is hence to introduce suitable quantities with a reduced number of degrees of freedom that are able to provide the desired spectra. A key quantity is the spectral function – see (1) – which can be calculated from the Green's function G:

$$A_{ii}(\omega) = \frac{1}{\pi}\left|\mathrm{Im}G_{ii}(\omega)\right|. \tag{4}$$

Many-body perturbation theory (MBPT) has traditionally been the framework in which different approaches have been developed to calculate G. We can refer to the various textbooks for a general introduction (see, e.g., [22–24]). Within MBPT, Hedin's *GW* approximation (*GW*A) [25] represents the state-of-the-art for the calculation of band structures in a large variety of materials. Besides the early review work by Hedin and Lundqvist [26], other in-depth reviews were published around the year 2000 [14, 27, 28]. Since then the number of applications has exploded, reaching more and more complicated materials such as interfaces [29], surfaces with adsorbates (see, e.g., [30–32]), or defects in bulk materials (see, e.g., [33–38]), and extending to other areas like quantum transport (see, e.g., [39–43]). Moreover, the field itself has experienced several advances, both from the technical and the fundamental points of view. For instance:

- Computational schemes that avoid sums of part or all the empty states have recently been proposed (see, e.g., [44–49]).
- Pathologies and limits of the *GW*A (e.g., the self-screening problem and the wrong atomic limit of the Hubbard model) and ways to go beyond *GW* have been explored (see, e.g., [34, 50–54]).
- The *GW*A has been extended in various ways to account for phenomena not contained in it. Examples include the cumulant expansion (see, e.g., [55, 56]), the T matrix approximation (see, e.g., [57–59]), approaches developed starting from the Hubbard model, like dynamical mean field theory (DMFT) [60], or with the calculation of vibrational excitations [61, 62].
- Another emerging research line in recent years has been the application of the *GW*A to non-equilibrium situations by means of the solution of the Baym–Kadanoff equations (see, e.g., [42, 63–65]).

In this chapter we will focus on the approaches that have been developed in the last decade to go beyond the perturbative G_0W_0 scheme (see Sect. 2), which has been the standard implementation for *GW* calculations in real materials. We will focus on the calculation of spectral properties (for instance we will not deal with calculations of ground-state total energies; see, e.g., [66–70]). While advanced computational schemes allow one to deal with more complicated materials (e.g., with a larger number of atoms), beyond-G_0W_0 approaches have led to a qualitative breakthrough in ab initio calculations of spectral properties of more complex materials, such as those containing localized *d* or *f* electrons, also including the challenging class of strongly correlated materials. In particular, in the following we will discuss why (see Sect. 3) and how (see Sects. 4 and 5) to go beyond G_0W_0, notably by means of the quasiparticle self-consistent *GW* (QS*GW*) method introduced in 2004 by Faleev et al. [71]. Finally, we will conclude the chapter by presenting a brief discussion of the new prospects that QS*GW* has opened in the field.

2 Theoretical Survival Kit in *GW* Environment

2.1 *Green's Function* G *and Self-Energy* Σ

The single-particle Green's function G is the most basic ingredient of MBPT. The time-ordered Green's function describes the propagation of an extra electron in an electronic system for positive times and the propagation of a missing electron (i.e., a hole) for negative times[1]:

[1] Here the spin degrees of freedom are omitted for simplicity. The generalization is however straightforward.

$$\begin{aligned} iG(\mathbf{r}t,\mathbf{r}'t') &= \theta\big(t-t'\big)\big\langle N0\big|\psi(\mathbf{r}t)\psi^{\dagger}(\mathbf{r}'t')\big|N0\big\rangle \\ &\quad -\theta(t'-t)\big\langle N0\big|\psi^{\dagger}(\mathbf{r}'t')\psi(\mathbf{r}t)\big|N0\big\rangle, \end{aligned} \tag{5}$$

where $|N0\rangle$ denotes the exact ground-state wavefunction of an N electron system, ψ and $\psi^{\dagger}$ are the annihilation/creation field operators in the Heisenberg picture, and θ is the step function.

The physical meaning of G becomes clear when inserting the closure relation in between the two field operators and taking a Fourier transform in time. The so-called Lehmann representation reads

$$G(\mathbf{r},\mathbf{r}',\omega) = \sum_i \frac{f_i(\mathbf{r})f_i^*(\mathbf{r}')}{\omega - E_i}. \tag{6}$$

The poles of G are located at the energies E_i:

$$\begin{aligned} E_i &= E_{N+1i} - E_{N0} - i\eta \quad \text{when } E_i > \mu \\ &= E_{N0} - E_{N-1i} + i\eta \quad \text{when } E_i < \mu, \end{aligned} \tag{7}$$

where the energies $E_{N\pm 1i}$ are the exact eigenenergies of the $N \pm 1$ electron system and i is the index labeling the exact eigenvectors of both the $N-1$ and $N+1$ electron systems. The ubiquitous vanishing positive η has naturally arisen from the Fourier transform of the step functions. In a solid, the discrete set of poles in (6) merges into a branch-cut. The so-called Lehmann amplitudes f_i are then defined as

$$\begin{aligned} f_i(\mathbf{r}) &= \big\langle N0\big|\psi(\mathbf{r}0)\big|N+1i\big\rangle \quad \text{when } E_i > \mu \\ &= \big\langle N-1i\big|\psi(\mathbf{r}0)\big|N0\big\rangle \quad \text{when } E_i < \mu. \end{aligned} \tag{8}$$

Note that the Lehmann amplitudes f_i are not mutually orthogonal. From this representation we see that the poles E_i carry the exact ionization energies of electrons in the system or the exact affinity energies. The analytical structure of G is also made clear: the poles lie slightly above the real axis for $E_i < \mu$ and slightly below for $E_i > \mu$. The poles can be directly compared to the peaks obtained from a photoemission or inverse photoemission experiment (see Sect. 1).

Because G is the fundamental quantity, a great deal of effort has been put in to its evaluation in a many-body context. This poses a very large challenge since equation of motion for G involves the two-particle Green's function. Its equation of motion in turn involves the three-particle Green's function, and so on. The standard remedy in MBPT is to break this hierarchy by introducing an effective operator, the self-energy Σ. As Schwinger showed, by introducing an auxiliary external field $U(\mathbf{r}t)$ that is set to zero at the end, it is possible to express formally the two-particle Green's function as a function of the one-particle Green's function [72]. This results in an equation of motion for G alone:

$$\int d\mathbf{r}'\{[\omega - h_0(\mathbf{r}) - V_{\mathrm{H}}(\mathbf{r})]\delta(\mathbf{r}-\mathbf{r}') - \Sigma(\mathbf{r},\mathbf{r}',\omega)\}G(\mathbf{r}',\mathbf{r}'',\omega) = \delta(\mathbf{r}-\mathbf{r}''). \quad (9)$$

Here h_0 is the non-interacting Hamiltonian and V_{H} the Hartree potential – see (3). Note that the self-energy Σ hides all the complexity of the original problem and thus is a non-local, dynamical and non-Hermitian operator. When $\Sigma = 0$ the Green's function G_0 is simply the resolvent of the Hartree Hamiltonian: $G_0^{-1} = \omega - h_0 - V_{\mathrm{H}}$. We refer the reader to the review articles of Strinati [72] or of Hedin and Lundqvist [26] for further details.

Dyson's equation results by multiplying (9) by G_0:

$$G(\mathbf{r},\mathbf{r}',\omega) = G_0(\mathbf{r},\mathbf{r}',\omega) + \int d\mathbf{r}_1 d\mathbf{r}_2 G_0(\mathbf{r},\mathbf{r}_1,\omega)\Sigma(\mathbf{r}_1,\mathbf{r}_2,\omega)G(\mathbf{r}_2,\mathbf{r}',\omega). \quad (10)$$

This equation establishes the link between the Hartree Green's function G_0 (easily calculated) and the fully interacting Green's function G (very hard to calculate) through the self-energy Σ.

The purpose of MBPT is then to provide approximations with increasing accuracy for the self-energy. The Coulomb interaction between electrons

$$v(\mathbf{r}-\mathbf{r}') = \frac{1}{|\mathbf{r}-\mathbf{r}'|} \quad (11)$$

is considered as the perturbation with respect to the independent-particle case. The first-order contribution to the self-energy is nothing else but the Fock exchange operator (the Hartree potential is already taken into account by G_0). This level of approximation is widely used for atoms and molecules, and in quantum chemistry perturbative methods in v with respect to Hartree–Fock are known as Møller–Plesset perturbation theory [73]. However, for the homogeneous electron gas, Hartree–Fock yields an anomalous zero density of states at the Fermi level. There is therefore a stringent need for higher order terms for periodic systems. Unfortunately, the analytical evaluation of one of the two second-order contributions is not finite in the case of the homogeneous electron gas [22, 23]. Perturbation theory is thus not justified. How should one proceed to circumvent this problem, especially for periodic systems?

2.2 *The Screened Coulomb Interaction* W

This divergence can be addressed in an effective manner by introducing a screened counterpart to the Coulomb interaction v. Other electrons act as a dielectric medium that reduces the interaction between any pair. It is common sense that the interaction between charges is not the same in vacuum as in a dielectric medium. At the macroscopic scale this is measured by the dielectric constant of the medium. At the microscopic scale the screening of the Coulomb interaction is given by

$$W(\mathbf{r},\mathbf{r}',\omega) = \int d\mathbf{r}_1 \varepsilon^{-1}(\mathbf{r},\mathbf{r}_1,\omega) v(\mathbf{r}_1 - \mathbf{r}'), \tag{12}$$

where the microscopic dielectric matrix ε^{-1} has been introduced. ε is linked to the macroscopic dielectric function ε_M [74, 75], which is a measurable quantity. For instance, $-\mathrm{Im}\varepsilon_M^{-1}$ is called the loss function and can be measured by electron energy loss spectroscopy (EELS) or inelastic X-ray scattering (IXS).

So far, the expression of the dielectric matrix has not been specified. Nevertheless, one can still analyze the physical meaning of the dynamically screened Coulomb interaction $W(\mathbf{r},\mathbf{r}',\omega)$. The effective interaction between electrons in a medium is decreased from v, the bare Coulomb interaction, to W the screened interaction. A perturbation theory based on W rather than on v then makes much more sense. However there is a price to pay: the screened interaction W is dynamical, meaning that the screening is more effective for some frequencies than for others. For metals, the static dielectric constant is infinite and consequently the long-range component of W vanishes. This fixes the problem of the vanishing density of states at the Fermi level predicted by Hartree–Fock theory for the homogeneous electron gas. Conversely, in the high frequency limit, the screening by the electrons becomes completely ineffective and the screened Coulomb interaction is simply the bare Coulomb interaction.

The additional complexity contained in W compared to v bears the hope that the perturbation theory is to be rapidly convergent. Maybe, as W already contains an infinite sum of interactions v, just the first order in W will suffice, as proposed by Hedin [25].

2.3 *Hedin's Equations and the* GW *Approximation*

Employing W instead of v in the MBPT allowed Hedin to reformulate the exact equations of the solution of the many-electron problem for the calculation of G [25]. They read:

$$G(1,2) = G_0(1,2) + \int d(34) G_0(1,3)\Sigma(3,4)G(4,2) \tag{13a}$$

$$\Sigma(1,2) = i\int d(34) G(1,3) W(1^+,4)\Gamma(3,2,4) \tag{13b}$$

$$W(1,2) = \int d(3)\varepsilon^{-1}(1,3)v(3,2) \tag{13c}$$

$$\varepsilon(1,2) = \delta(1,2) - \int d(3) v(1,3)\tilde{\chi}(3,2) \tag{13d}$$

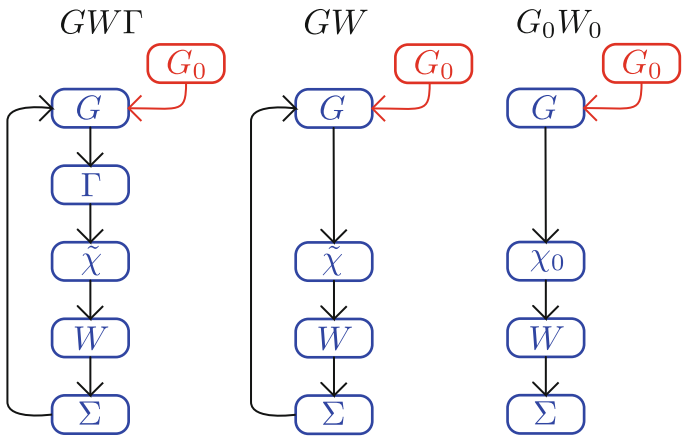

Fig. 2 Schematic view of the three frameworks described in this review. The exact expression ($GW\Gamma$, *left panel*) can be obtained after an initialization with a guessed Green's function G_0 by iteration of all the Hedin's equations. The self-consistent GW approximation (GW, *central panel*) arises from the iteration of the equations keeping the vertex function $\Gamma = 1$. The perturbative GW approximation (G_0W_0, *right panel*) is the one-shot evaluation of the GW self-energy based on the guessed Green's function G_0

$$\widetilde{\chi}(1,2) = -i\int d(34)G(1,3)G(4,1)\Gamma(3,4,2) \tag{13e}$$

$$\Gamma(1,2,3) = \delta(1,2)\delta(1,3) + \int d(4567)\frac{\delta\Sigma(1,2)}{\delta G(4,5)}G(4,6)G(7,5)\Gamma(6,7,3). \tag{13f}$$

Contracted indexes $(1) = (\mathbf{r}_1,t_1,\sigma_1)$ have been used for simplification. The index 1^+ denotes the times $t_1 + \eta$ for a vanishing positive η. Most of the quantities have been introduced earlier. $\widetilde{\chi}$ is the irreducible polarizability and Γ is the three-point vertex function. These nonlinear equations are coupled. If solved self-consistently, these equations form an exact scheme to obtain the solution of the many-body problem. This process is pictured in the left panel of Fig. 2. Of course, in practice, even in the simplest cases it is not feasible, mainly due to the presence of the three-point vertex function Γ. It is then natural that an approximated scheme begins by simplifying this particular term.

The second term in the right-hand side of (13f) involves the self-energy which is of first-order in W according to (13b). Retaining only the zero-order terms in (13f) (i.e., the δ functions), Hedin's equations are greatly simplified:

$$G(1,2) = G_0(1,2) + \int d(34)G_0(1,3)\Sigma(3,4)G(4,2) \tag{14a}$$

$$\Sigma(1,2) = iG(1,2)W(1^+,2) \tag{14b}$$

$$W(1,2) = \int d(3)\varepsilon^{-1}(1,3)v(3,2) \tag{14c}$$

$$\varepsilon(1,2) = \delta(1,2) - \int d(3)v(1,3)\widetilde{\chi}(3,2) \tag{14d}$$

$$\widetilde{\chi}(1,2) = -iG(1,2)G(2,1). \tag{14e}$$

The irreducible polarizability $\widetilde{\chi}$ is then a simple product of two Green's functions. This is the well known Random-Phase Approximation (RPA) to the dielectric matrix. The self-energy is also much simplified: this is just the simple product of G and W, giving the name to the *GW* approximation. It is of first-order in W. The missing terms (second and higher orders in W) are commonly named the "vertex corrections".

The set of equations (14a–14e) still requires a self-consistent treatment since W and Σ depend on G, which is the quantity one needs to find. This is pictured in the central panel of Fig. 2. The practical implementation of these equations is still far from obvious. This is the reason why for many years the *GW* self-energy has been evaluated non-self-consistently.

2.4 *Practical Calculation of the GW Self-Energy: The* G_0W_0 *Approach*

It is usually impossible to evaluate the Green's function self-consistently from (14a–14e). However, let us imagine that mean-field theories such as Hartree–Fock or Kohn–Sham provide a good description of the electronic system under study. In a mean-field theory, the one-electron wavefunctions $\phi_i(\mathbf{r})$ and eigenvalues ε_i allow one to evaluate the independent-particle Green's function[2] G_0

$$G_0(\mathbf{r},\mathbf{r}',\omega) = \sum_i \frac{\phi_i(\mathbf{r})\phi_i^*(\mathbf{r}')}{\omega - \varepsilon_i + i\eta \mathrm{sign}(\varepsilon_i - \mu)}. \tag{15}$$

The location of the poles of G_0 are above the real axis for occupied states and below for empty states. As a consequence, $\widetilde{\chi}$ and then W can be readily evaluated from this expression of G_0. Let us label this evaluation of the irreducible polarizability χ_0 and of the screened Coulomb interaction, W_0. Finally, the *GW* self-energy is obtained as the convolution G_0W_0.

[2] G_0 here can be understood as a generalization of the Hartree Green's function introduced in (10.2), and thus we keep the same notation for a distinct quantity. See also Sect. 2.1 for an extended discussion.

The so-called G_0W_0 approach consists in stopping the procedure immediately after the first evaluation of the self-energy, as shown in the right hand panel of Fig. 2. This "one-shot" procedure is justified when the starting mean-field theory used for G_0 is accurate enough for the targeted property. The vast majority of the *GW* applications for almost 50 years have been obtained with the G_0W_0 procedure. Of course, the choice of the starting point is material dependent. The seminal paper of Hedin [25] simply employed the free electron model to calculate the *GW* self-energy for the homogeneous electron gas. The first application of *GW* to real solids used either the Hartree–Fock approximation [76] or the local density approximation [77]. For atoms, Shirley and Martin chose Hartree–Fock [78]. The rationale underlying the choice is the selection of the most accurate mean-field theory for the specific system under scrutiny. This strategy is sometimes referred to as the "best *G*, best *W*" approach (see Sect. 3.1).

In the quasiparticle approximation, the Dyson equation (10) becomes

$$\left(-\frac{\nabla^2}{2}+V_{\text{ext}}(\mathbf{r})+V_{\text{H}}(\mathbf{r})\right)\psi_i(\mathbf{r})+\int d\mathbf{r}'\,\Sigma\big(\mathbf{r},\mathbf{r}',E_i\big)\psi_i(\mathbf{r}')=E_i\psi_i(\mathbf{r}) \tag{16}$$

In the G_0W_0 framework one assumes that the quasiparticle wavefunctions ψ_i can be approximated by the Kohn–Sham orbitals ϕ_i. By comparing (3) and (16) one finds that the quasiparticle energies E_i can be calculated as a first-order correction with respect to the underlying mean-field starting point from

$$E_i=\varepsilon_i+\big\langle\phi_i\big|\Sigma(E_i)-V_{\text{xc}}\big|\phi_i\big\rangle, \tag{17}$$

where Σ is the G_0W_0 self-energy. From a linearization of the frequency dependence of Σ, one finally obtains

$$E_i=\varepsilon_i+Z_i\big\langle\phi_i\big|\Sigma(\varepsilon_i)-V_{\text{xc}}\big|\phi_i\big\rangle, \tag{18}$$

where the renormalization factors Z_i are

$$Z_i=\left[1-\langle\phi_i\big|\frac{\partial\Sigma(\omega)}{\partial\omega}\big|_{\omega=\varepsilon_i}\big|\phi_i\rangle\right]^{-1}. \tag{19}$$

In most G_0W_0 calculations the band structures are obtained using (18). One can also calculate the spectral function defined in (4) from:

$$A_{ii}(\omega)=\frac{1}{\pi}\frac{\big|\big\langle\phi_i\big|\text{Im}\Sigma(\omega)\big|\phi_i\big\rangle\big|}{\big[\omega-\varepsilon_i-\big\langle\phi_i\big|\text{Re}\Sigma(\omega)-V_{\text{xc}}\big|\phi_i\big\rangle\big]^2+\big[\big\langle\phi_i\big|\text{Im}\Sigma(\omega)\big|\phi_i\big\rangle\big]^2}. \tag{20}$$

The spectral function has poles correspondence to the quasiparticle energies, i.e., when $\omega-\varepsilon_i-\langle\phi_i|\text{Re}\Sigma(\omega)-V_{\text{xc}}|\phi_i\rangle=0$; cf. (17). The width of the quasiparticle peak is given by $\text{Im}\Sigma(\omega)$, which is hence linked to the lifetime of the excitation (defined as the inverse of its width). The spectral function can have other peaks, the

satellites, that originate from structures in $\mathrm{Im}\Sigma(\omega)$. $\omega - \varepsilon_i - \langle\phi_i|\mathrm{Re}\Sigma(\omega) - V_{xc}|\phi_i\rangle$ can also have additional zeroes, giving rise to satellites. Within the *GW*A this latter kind of satellites has been called plasmarons [79, 80], but lately they have been shown to be an artifact of the *GW*A [56, 81, 82]. In Hartree–Fock the self-energy is Hermitian: $\mathrm{Im}\Sigma(\omega) = 0$. Therefore quasiparticle peaks become delta functions (i.e., the lifetime of quasiparticle becomes infinite). Moreover, since the self-energy is static, no other structures (e.g., satellites) can appear in the spectral function.

The *GW* self-energy can be split into a Fock exchange term Σ_x and a correlation term $\Sigma_c(\omega)$: $\Sigma(\omega) = \Sigma_x + \Sigma_c(\omega)$. While $\Sigma_x = iGv$ is static, the evaluation of $\Sigma_c(\omega)$ requires the calculation of the convolution integral of G and $W_p = W - v$:

$$\Sigma_c(\mathbf{r}_1, \mathbf{r}_2, \omega) = \frac{i}{2\pi}\int d\omega' e^{i\eta\omega'} G\left(\mathbf{r}_1, \mathbf{r}_2, \omega + \omega'\right) W_p\left(\mathbf{r}_1, \mathbf{r}_2, \omega'\right). \tag{21}$$

Since Σ_c is obtained through the frequency integration (21), the fine details of the energy dependence of W_p are often not important. In these cases one can approximate the imaginary part of the inverse dielectric function ε^{-1} as a single-pole function in ω (plasmon-pole model) [83, 84]. Plasmon-pole models can be used for calculating quasiparticle energies, but should be avoided for spectral functions because, for example, they do not describe $\mathrm{Im}\Sigma$ correctly. In these cases the full-frequency dependence of Σ is required and the frequency integration has to be performed with care [85].

The spectral representation of W_p is given by [5]

$$W_p(\mathbf{r}_1, \mathbf{r}_2, \omega) = 2\sum_s \frac{\omega_s W_s(\mathbf{r}_1, \mathbf{r}_2)}{\omega^2 - (\omega_s - i\eta)^2}. \tag{22}$$

The poles of W_p are the energies ω_s that correspond to neutral excitations (electron-hole transitions and plasmons). By combining (22) with (15) and performing the frequency integration (21), one finds that the G_0W_0 self-energy is given by the sum of two terms:

$$\Sigma_{\mathrm{SEX}}(\mathbf{r}_1, \mathbf{r}_2, \omega) = -\sum_i \theta(\mu - \varepsilon_i)\phi_i(\mathbf{r}_1)\phi_i^*(\mathbf{r}_2) W(\mathbf{r}_1, \mathbf{r}_2, \omega - \varepsilon_i), \tag{23a}$$

$$\Sigma_{\mathrm{COH}}(\mathbf{r}_1, \mathbf{r}_2, \omega) = \sum_i \phi_i(\mathbf{r}_1)\phi_i^*(\mathbf{r}_2)\sum_s \frac{W_s(\mathbf{r}_1, \mathbf{r}_2)}{\omega - (\omega_s - i\eta) - \varepsilon_i}. \tag{23b}$$

The first term arises from the poles in G and the second from the poles in W. Owing to the similarity of the first term with the Fock exchange, it is usually called the "screened exchange" term. The second term is referred to as the "Coulomb-hole" term [25]. If a further static approximation is carried out, this decomposition gives rise to the so-called COHSEX (Coulomb hole plus screened exchange), first introduced by Hedin [25, 79]. This static and Hermitian self-energy is obtained by setting $\omega - \varepsilon_i = 0$ in $\Sigma_{\mathrm{SEX}}(\omega)$ and $\Sigma_{\mathrm{COH}}(\omega)$. This corresponds to assuming that the

main contribution to the self-energy $\Sigma(\omega)$ stems from the states ε_i close to ω. So $\omega - \varepsilon_i$ is small compared to the main excitations in W which are at the plasmon energies ω_s [25, 79].

In the majority of practical cases the G_0W_0 scheme is largely sufficient to evaluate successfully the GW self-energy. However for some cases it is not. This review will focus precisely on those pathological cases.

3 Beyond G_0W_0

In this section we will present arguments to show why one should go beyond the G_0W_0 scheme that has been introduced in the previous section. First of all, we will discuss the criticisms that can be raised about G_0W_0 from the point of view of *basic principles*. Then we will consider a case study where the G_0W_0 scheme shows *in practice* to be inadequate under different aspects. This practical example is VO_2, a prototypical transition metal oxide, which has been the subject of an intense debate for the last 5 decades for its metal-insulator transition occurring just above room temperature [86].

3.1 Which Starting Point?

The GW approximation can be seen to correspond to the first step of an iterative solution of Hedin's equations that takes as the starting point $\Sigma = 0$ (see Fig. 2). Therefore, in principle the GW self-energy should be built using a Green's function G calculated in the Hartree approximation (i.e., with $\Sigma = 0$). However, the Hartree approximation is generally inadequate, giving bad electron densities and one-particle wavefunctions. Moreover, performing an additional step in the iterative solution of Hedin's equations leads to the inclusion of vertex corrections beyond GW that are immediately very expensive from the computational point of view.

One would rather like to remain within the GWA and find an alternative strategy to evaluate the self-energy, discarding the idea of solving Hedin's equations iteratively. This has been the approach followed in practice in the application of the GWA to the calculations of band structures of real materials [18, 77, 83]. The idea is to build the GW self-energy with the best ingredients that can be calculated from first-principles. Historically, in solids this led to the use of the LDA or the GGA (alternatively, Hartree–Fock for atoms [78]) at the place of the Hartree approximation. This was justified by the observation that in *sp* semiconductors and metals LDA wavefunctions are a good approximation to QP wavefunctions [83] (see Sect. 2.4). A posteriori this choice was validated by the good agreement of G_0W_0 results with experimental band gaps [27, 28].

Moreover, still in the spirit of the iterative solution of Hedin's equations, one could improve the starting point by setting $\Sigma = V_{xc}$, instead of $\Sigma = 0$ [83, 87]. This would give a self-energy that still has a *GW*-like form. However, the Coulomb interaction is now screened by an effective dielectric function that has a electron-test-charge form, $\widetilde{\varepsilon} = 1 - (v + f_{xc})\chi_0$, instead of the RPA ε used in the standard *GW* approximation, $\varepsilon = 1 - v\chi_0$. The main difference is that in the electron-test-charge case the induced charge generates an exchange-correlation potential in addition to the induced Coulomb potential that is already taken into account at the RPA level. This approximation has been called "*GW*Γ" [87] because it contains, to some extent, vertex corrections beyond *GW*. It is consistently derived and calculated using Kohn–Sham ingredients. It has been shown to give results that are similar to (or slightly worse than) standard LDA-based *GW* [29, 52, 87, 88], adding another argument in favor of the pragmatic "best G best W" approach. Vertex corrections beyond the local approximation used to build vertex in the "*GW*Γ" scheme [87] are still an open question under investigation [89, 90].

Anyway, this "best G best W" strategy clearly introduces a degree of arbitrariness in the results. As any first-order perturbation scheme, the G_0W_0 results directly depend on the quality of the starting point (i.e., the zero order of the perturbative scheme). In general, Hartree–Fock overestimates and the LDA (or GGA) underestimates band gaps (and analogously HOMO-LUMO gaps in finite systems). G_0W_0 corrections improve with respect to the starting point, getting closer to experiment from above if starting from Hartree–Fock, or from below if starting from LDA or GGA. Therefore G_0W_0 results obtained from these two starting points generally bracket the reference values, and starting from any hybrid functional mixing LDA with Fock non-local exchange gives rise to intermediate results between the two. This observation is, for instance, illustrated for a benchmark of 34 small closed-shell molecules in Fig. 3. Deviations from the reference quantum chemistry CCSD(T) calculations are reported: each bar corresponds to a different approximation for the exchange-correlation functional used in the underlying mean-field calculation, comprising local, semilocal, and several hybrid functionals [92]. Similar results for atoms and molecules have recently been obtained, for instance also in [91, 93–96], and these observations can be generalized to extended systems as well.

Moreover, in contrast to the first applications of the LDA-based G_0W_0 scheme, in recent years the investigation of more complex materials has shown severe limitations of the G_0W_0 approach. Alternative starting points beyond LDA have been put forward, either remaining in the Kohn–Sham scheme – e.g., using the exact exchange approximation (EXX) [97, 98] or LDA+U [99, 100] – or moving to a generalized Kohn–Sham scheme and adding a part of non-local Fock exchange – e.g., using the Heyd–Scuseria–Ernzerhof (HSE) hybrid functional [101, 102]. In most cases bad G_0W_0 results have been explained in terms of the inadequacy of the underlying LDA starting point.

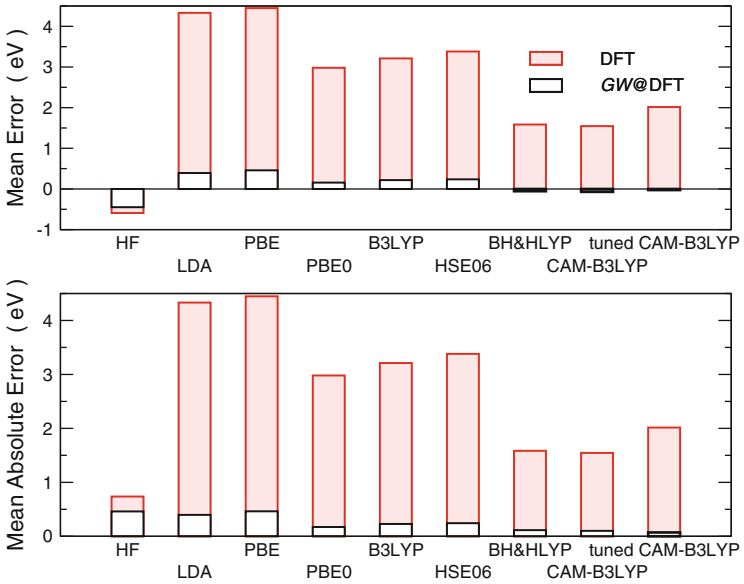

Fig. 3 Deviation of the HOMO energies with respect to the CCSD(T) total energy difference. The *upper panel* shows the mean error (ME), and the *lower panel* the mean-absolute error (MAE) for the 34-molecule set introduced in [91]. The *shaded bar* corresponds to the HOMO energy of the starting point, and the *white bar* shows the corresponding G_0W_0 HOMO energy. Reprinted with permission from [92]. Copyright 2013, American Chemical Society

3.2 Energy Scales

In the G_0W_0 scheme, the self-energy displays a dependency on the absolute energy scale used for the construction of G_0. To illustrate this statement we follow Hedin [5, 25] and we introduce an arbitrary shift Δ of the energy scale of G_0. The Green's function G_0^{Δ}, depending parametrically on Δ, can be written as (see (15))

$$G_0^{\Delta}(\mathbf{r}_1, \mathbf{r}_2, \omega) = \sum_i \frac{\phi_i(\mathbf{r}_1)\phi_i^*(\mathbf{r}_2)}{\omega - \varepsilon_i - \Delta + i\eta \mathrm{sgn}(\varepsilon_i - \mu)} \tag{24}$$

While χ_0 and W_0 are independent of Δ, the G_0W_0 self-energy becomes

$$\Sigma^{\Delta}(\omega) = \Sigma^{\Delta=0}(\omega - \Delta). \tag{25}$$

Using the linear expansion of $\Sigma^{\Delta}(\omega)$ – see (18) – the quasiparticle energies are in turn calculated as

$$E_i = \varepsilon_i + \Delta + Z_i^{\Delta=0}\left[\left\langle \phi_i \middle| \Sigma^{\Delta=0}(\varepsilon_i) - V_{\mathrm{xc}} \middle| \phi_i \right\rangle - \Delta\right]. \tag{26}$$

The result should not depend on the absolute energy scale, which is arbitrary.

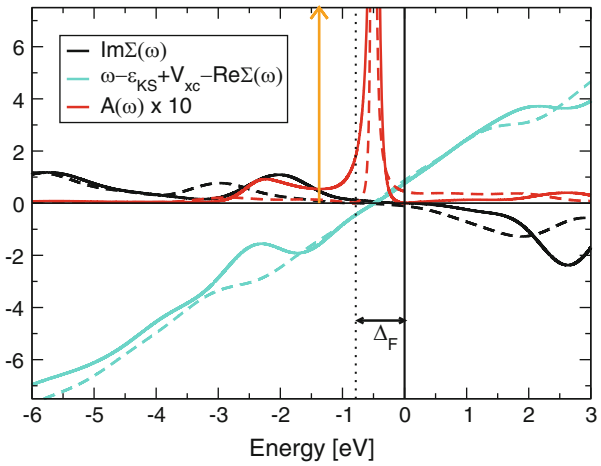

Fig. 4 Spectral functions $A(\omega)$ and self-energy $\Sigma(\omega)$ for the top-valence state at Γ point for the metallic phase of VO_2, calculated in G_0W_0 (*dashed lines*) and eigenvalue self-consistent *GW* (*solid lines*). *Vertical orange arrow*: energy of the LDA KS state. *Vertical dotted line*: Fermi energy in LDA. The zero of the energy axis is at the Fermi energy calculated in the eigenvalue self-consistent *GW*. Δ_F is the shift of the Fermi energy. From Gatti et al. (2013) Unpublished

On the contrary, here we see that shifting by Δ the energy scale of G_0 leads to a variation of the quasiparticle energies equal to $(1 - Z_i^{\Delta=0})\Delta$. This is a consequence of the fact that the self-energy in the *GW*A is dynamical, hence $Z_i \neq 1$.

However, if the renormalization factors Z_i do not change much from state to state, as is generally the case in simple systems, this dependency on the absolute energy scale of G_0 has a tiny effect on the G_0W_0 band-structure results. In this situation, in fact, changing arbitrarily the energy scale of G_0 would only give a rigid shift of the whole band structure.

In order to fix this problem, Hedin suggested setting the energy scale by requiring a self-consistency at the Fermi level [5, 25]. This means setting Δ equal to the matrix element of the self-energy at the Fermi level calculated with $\Delta = 0$. A more general solution would be to calculate self-consistently the energies entering Σ (and hence also the Fermi level).

A more severe consequence of this dependency on the energy scale can be found in the calculation of spectral functions. To see this effect in practice, we consider here the example of the metallic phase of VO_2 [Gatti et al. (2013) Unpublished]. In Fig. 4 we compare the spectral functions calculated within G_0W_0 (dashed lines) and within a scheme in which the quasiparticle energies used to calculate the *GW* self-energy are updated to self-consistency (solid lines). In LDA the spectral function for each state is just a delta peak and in Fig. 4 the LDA top valence at the Γ point is represented by the vertical arrow. It corresponds to a V 3d state. In G_0W_0 the corresponding position of the quasiparticle peak is shifted upwards and its width becomes finite, meaning a finite lifetime of the quasiparticle excitation. The shift of the peaks is similar for all the other V 3d states (not shown in Fig. 4), which also

have very similar renormalization factors. This is the situation described above: the absolute energy scale entering G_0 does not have an important influence on the band-structure results.

On the contrary, G_0W_0 gives an inaccurate description of the incoherent features (i.e., besides the quasiparticle peak) in the spectral function. In fact, the satellite measured in the photoemission spectrum of metallic VO_2 [103] is too weak in the G_0W_0 spectral function (see dashed red line in Fig. 4)) [104]. On the basis of this G_0W_0 result, one would claim the inadequacy of the GW approximation for the description of this genuine signature of dynamical correlation. However, we now show that it is actually a problem of the G_0W_0 scheme itself.

In G_0W_0 the energy scale for G_0 is given by the LDA starting point. For example, the imaginary part of the G_0W_0 self-energy can be written as (see (15), (21), and (22))

$$\mathrm{Im}\Sigma(\mathbf{r},\mathbf{r}',\omega) = \mathrm{sgn}(\mu-\varepsilon_i)\pi\sum_{i,s\neq 0}\phi_i(\mathbf{r})\phi_i^*(\mathbf{r}')W_s(\mathbf{r},\mathbf{r}')\delta[\omega-\varepsilon_i+\omega_s\mathrm{sgn}(\mu-\varepsilon_i)] \tag{27}$$

where ε_i are LDA energies and μ the LDA Fermi energy. Therefore, the G_0W_0 $\mathrm{Im}\Sigma(\omega)$ (see dashed black line in Fig. 4) changes its sign, crossing zero at the LDA Fermi energy (vertical dotted line in Fig. 4) which does not correspond to the Fermi energy after inclusion of GW corrections. In the eigenvalue self-consistent GW scheme, instead, since the energies ε_i entering the self-energy are updated self-consistently, $\mathrm{Im}\Sigma(\omega)$ (solid black line), as expected, crosses zero at the Fermi energy μ that is obtained self-consistently (zero of energy axis in Fig. 4).

The peaks in $\mathrm{Im}\Sigma(\omega)$ can give rise to structures (satellites) in the spectral function; see (20). This is indeed the case for the top-valence state of VO_2 in Fig. 4. For occupied states peaks of $\mathrm{Im}\Sigma(\omega)$ are located approximately at $-\omega_s+\varepsilon_i$; see (27). In VO_2 $\omega_s\sim$1.5 eV is the energy of a localized $d-d$ plasmon and the coupling with this plasmon is at the origin of the satellite [105]. This satellite is called a shake-up excitation. This means that in the photoemission process the photoemitted electron leaves the $(N-1)$-electron system in an excited state in which the creation of an additional plasmon excitation has occurred. The main QP peak in this case corresponds to the ground state of the $(N-1)$-electron system.

On the basis of this physical picture, for the energy-conservation rule we expect that in the spectral function the satellite is at lower energy than the quasiparticle peak and the distance is equal to the plasmon energy ω_s. However, this does not happen in G_0W_0 approximation. In fact, in G_0W_0 the QP energy is shifted upwards with respect to the LDA energy ε_i that is used to build $\mathrm{Im}\Sigma_i$. If we call this shift Δ_i, from (27) we find that the peak of $\mathrm{Im}\Sigma_i$ is located at $-\omega_s+\varepsilon_i$ and hence has a distance $\Delta_i+\omega_s$ from the QP peak. Since $\Delta_i>0$, the satellite in G_0W_0 has then too high a binding energy. Moreover, the intensity is so weak that one would even

conclude that there is no satellite in *GW* [104]. Instead, in the eigenvalue self-consistent *GW* scheme the satellite gets closer to the QP peak (see solid red line), because at self-consistency $\Delta_i = 0$. The distance between the satellite and the QP peak becomes correctly $\sim \omega_s$, i.e., the energy of the plasmon. Moreover, the intensity of the satellite is enhanced with respect to G_0W_0 due to the fact that $|(\omega - \varepsilon_i - (\mathrm{Re}\Sigma_i(\omega) - V_i^{\mathrm{xc}})|$ becomes smaller (compare solid and dashed cyan lines). In conclusion, the eigenvalue-self-consistent *GW* scheme gives a correct description of the low-energy satellite [Gatti et al. (2013) Unpublished], in contrast to G_0W_0.

The example just discussed shows that conclusions about spectral functions should not be based on calculations at the G_0W_0 level, especially if one is interested in spectral properties close to the Fermi level and the self-energy induces a non-negligible shift of the positions of the peaks with respect to the LDA starting point. In fact the same problem has been observed in other situations, such as Hubbard chains [106] or $SrVO_3$, another prototypical strongly correlated metal [107]. This conclusion is also relevant when *GW* is combined with other methods that calculate spectral functions, such as dynamical mean field theory (DMFT).

3.3 Quasiparticle Wavefunctions

The G_0W_0 scheme is based on the hypothesis that QP wavefunctions can be approximated by LDA orbitals; see (17). This assumption holds for simple semiconductors and metals and has been investigated in depth, e.g., for bulk silicon [83]. However, it has been known for a long time that it can be questionable for finite systems [108] and surfaces [109–111]. In simple systems like bulk silicon the LDA conduction wave functions have also recently been shown to be of significantly poorer quality, in particular away from highly symmetric points of the Brillouin zone [112]. Here, through the case study of the insulating phase of VO_2, we discuss a situation in which the G_0W_0 perturbation theory breaks down completely [105]. Similar problems occur when LDA produces a wrong ordering of the bands (see, e.g., [113, 114]).

Across the metal-insulator transition, VO_2 also undergoes a structural phase transition from rutile (metal) to monoclinic (insulator). This is accompanied by the formation of V–V dimers along the rutile *c* axis, resulting into a doubling of the unit cell. The LDA underestimates the bonding-antibonding splitting of the V 3*d* states associated with the formation of these V–V dimers and in turn the band structure is metallic [115]. Alternatively, the metallic LDA band structure has been interpreted as the proof of the strongly correlated nature of VO_2 [116].

In apparent support of the hypothesis of "strong correlation," G_0W_0 based on LDA also fails to open the gap. In order to get rid of the LDA starting point, QP wavefunctions have been calculated self-consistently in the COHSEX approximation [105]. This self-consistent quasiparticle calculation does succeed in opening a

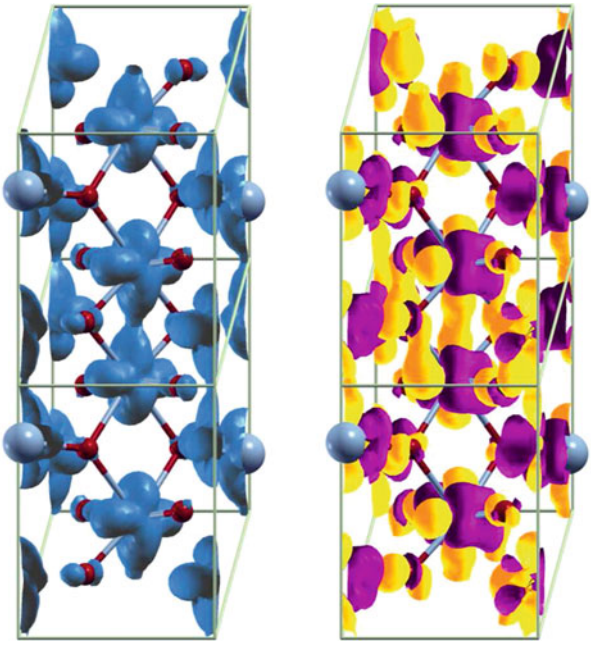

Fig. 5 (*Left panel*) Isosurface of the LDA electron density for the top valence V 3d bands in insulating VO_2. It is a V–V dimer bonding a_{1g} state, highly polarized along the *cc* axis (*vertical axis* in the figure). (*Right panel*) Difference between COHSEX and LDA electron density for the same states. *Yellow surfaces* are for positive variations and *purple* for negative ones. The *c*-axis polarization increases for COHSEX wavefunctions. See [105]

gap (0.8 eV, quite close to the experimental value of 0.6 eV). In contrast, in a COHSEX calculation where the wavefunctions are constrained to be the LDA ones and only the energies are updated self-consistently, a gap close to zero is found: the change of the wavefunctions with respect to the LDA ones is thus of utmost importance.

In Fig. 5 the LDA electron density for the top valence bands is plotted (see the left panel). It represents the V a_{1g} states that derive from the V–V dimer bonding states and are hence highly polarized along the V–V dimer axis (the vertical *c* axis in the figure). The self-consistent QP COHSEX calculation results in the enhancement of this anisotropy, inducing a stronger bonding character to the top valence wavefunctions. Therefore if the orbital redistribution associated with the formation of V–V dimers is underestimated, as happens in LDA, the system remains metallic. Since LDA orbitals are not a sufficiently good approximation of the QP wavefunctions at the Fermi level, the G_0W_0 perturbative scheme on top of LDA is not valid in the present situation. Improved QP wavefunctions are instead obtained in the COHSEX approximation, which can be used for a subsequent G_0W_0 calculation.

More generally, this conclusion about the failure of G_0W_0 holds for *d* and *f* electron states for which the LDA tends to produce too delocalized wavefunctions [71, 113, 117–126]. The Fock exchange term of the self-energy is essential in these situations to cure this delocalization error [126].

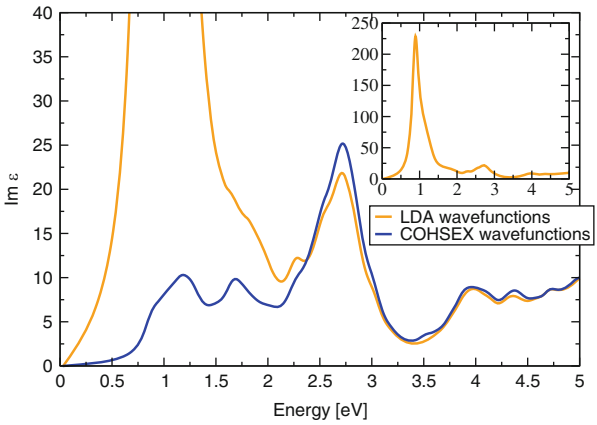

Fig. 6 Absorption spectrum Im ϵ of insulating VO_2, calculated in the independent-particle approximation using COHSEX+ G_0W_0 energies and LDA (*yellow line* in the *main panel* and in the *inset*) or COHSEX (*blue line*) wavefunctions. See Gatti et al. (2013) Unpublished

Finally, in Fig. 6 we illustrate the effect of using QP wavefunctions instead of LDA ones in the optical spectra of insulating VO_2 [Gatti et al. (2013) Unpublished]. Here the absorption spectrum, given by the imaginary part of the dielectric function ε_M, is obtained as a sum over independent vertical transitions from valence to conduction states, corresponding to Fermi's golden rule in the independent-particle picture. The energies of these transition are calculated using the COHSEX+ G_0W_0 results that correctly produce an insulator in VO_2 [105]; hence the onset of the optical spectrum is at a finite energy. However, the spectrum calculated with LDA wavefunctions starts with a peak of huge intensity (see yellow line). This huge peak derives from the shift of the metallic Drude peak at $\omega \sim 0$ in the spectrum calculated with metallic LDA eigenvalues. In order to understand this problem better, we write the oscillators strengths for vanishing $\mathbf{q}$ that determine the absorption spectrum by using $\mathbf{k} \cdot \mathbf{p}$ perturbation theory [127]:

$$\lim_{\mathbf{q}\to 0} \left\langle \phi_{v\mathbf{k}} \middle| e^{-i\mathbf{q}\cdot\mathbf{r}} \middle| \phi_{c\mathbf{k}+\mathbf{q}} \right\rangle = \lim_{\mathbf{q}\to 0} \frac{i\mathbf{q} \cdot \left\langle \phi_{v\mathbf{k}} \middle| \left[H^{\mathrm{KS}}, \mathbf{r} \right] \middle| \phi_{c\mathbf{k}} \right\rangle}{\varepsilon_{c\mathbf{k}} - \varepsilon_{v\mathbf{k}}}, \tag{28}$$

with $H^{\mathrm{KS}}\phi_i = \varepsilon_i\phi_i$. If LDA wavefunctions are used to calculate the oscillator strengths (28), then the energy differences appearing at the denominator in (28) are by definition also to be calculated in LDA. Therefore, since VO_2 is metallic in LDA, for the first transitions the denominator is vanishingly small. In turn, the oscillator strength of the first peak remains very high, although the *position* is given correctly by COHSEX+ G_0W_0 energy differences. Thus the wrong oscillator strength is due to the use of LDA wavefunctions and is corrected by using QP wavefunctions calculated in the self-consistent COHSEX scheme (see blue line in Fig. 6). The effect is drastic for VO_2, but one should expect similar behavior whenever the opening of a small bandgap is accompanied by a change of wavefunctions.

4 Quasiparticle Self-Consistent *GW*

For all the aforementioned reasons, it seems very attractive to get rid of the mean-field starting point which pervasively affects all the G_0W_0 results. The natural way to do so would be to turn to self-consistent *GW* calculations, as pictured in the central panel of Fig. 2. However, the full self-consistent *GW* approach suffers from many drawbacks as we will show in the next paragraph. This is the main reason why Faleev, Kotani, and van Schilfgaarde introduced in 2004 the so-called "Quasiparticle-Self-consistent *GW*" scheme [71], to which this section is devoted.

4.1 Full Self-Consistent GW

The full self-consistent *GW* is affected by two kinds of issues: there are some well identified theoretical problems and the calculations are extremely cumbersome.

In the self-consistent *GW* scheme, the Dyson equation (10) is solved self-consistently using the *GW* self-energy. At first sight, self-consistent *GW* is appealing, since it is a conserving approximation, obeying conservation laws for particle number, energy, and momentum under the influence of external perturbations [129]. For instance, it has been shown to yield very accurate total energies [68, 69]. However, in self-consistent *GW* the polarizability $\widetilde{\chi}$ is built from the interacting Green's functions G that contain dynamical self-energy effects. In contrast to G_0, the spectrum of the full Green's function G contains not only quasiparticles but also "incoherent" parts with a finite spectral weight. This transfer of spectral weight is measured by the renormalization factor Z, which is most often smaller than 1. When performing self-consistent *GW* without any vertex correction, the polarizability $\widetilde{\chi} = -iGG$ contains excitations renormalized with a factor Z^2 [118]. As a consequence, screening is reduced and the results are worse in practice. Furthermore, the resulting polarizability $\widetilde{\chi}$ does not obey the f-sum rule [67]. To summarize, there are theoretical arguments that strongly hint towards the inclusion of both self-consistency and vertex corrections together [130, 131].

These problems do not appear to be too dramatic for atoms and molecules. For finite systems, self-consistent *GW* does not deteriorate G_0W_0 results [93, 95, 132] since, in this case, the dynamical effects in Σ are indeed negligible (i.e., $Z \sim 1$). However, as far as we are interested in solid-state systems, the full self-consistent approach appears to be questionable.

Besides these physical problems, the computational cost of self-consistent *GW* is very high. The *GW* self-energy is dynamical: the equations have a frequency dependence. For instance, the quasiparticle wavefunctions are not eigenvectors of the same Hamiltonian. The *GW* self-energy is non-Hermitian: one should distinguish left and right eigenvectors and the eigenvalues are complex. As a

consequence, the "wavefunctions" do not form an orthogonal basis. In summary, a fully self-consistent *GW* calculation is a formidable task and one can easily appreciate why its application to solid-state systems has been so scarce in the available literature.

4.2 The QSGW Approximation to the GW Self-Energy

A static and Hermitian approximation to the *GW* self-energy would be devoid of the issues mentioned in the previous paragraph. This would prevent the spectral weight from being transferred to the "incoherent part," then curing most the physical flaws of the self-consistent *GW* scheme. Furthermore, it would allow one to have an orthogonal set of wavefunctions that are eigenvectors of the same (non-local) Hamiltonian. The computational gain would be massive.

The problem is then to design a static and Hermitian approximation that still retains the accuracy of the full *GW* self-energy. Faleev, Kotani, and van Schilfgaarde made two proposals in their seminal paper of 2004 [71]. One method was identified as clearly superior to the other: this is the method nowadays named QS*GW*. The matrix elements of the self-energy in the QS*GW* approximation read

$$\begin{aligned}\left\langle \psi_i \middle| \Sigma^{\mathrm{QS}GW} \middle| \psi_j \right\rangle = \frac{1}{4}\Big\{ &\left\langle \psi_i \middle| \Sigma^{GW}(E_i) \middle| \psi_j \right\rangle + \left\langle \psi_j \middle| \Sigma^{GW}(E_i) \middle| \psi_i \right\rangle^* \\ &+ \left\langle \psi_i \middle| \Sigma^{GW}(E_j) \middle| \psi_j \right\rangle + \left\langle \psi_j \middle| \Sigma^{GW}(E_j) \middle| \psi_i \right\rangle^* \Big\}.\end{aligned} \tag{29}$$

The QS*GW* method was later justified as a way to optimize the quasiparticle Hamiltonian H_0 with respect to $\Delta(\omega) = H(\omega) - H_0$, where $H(\omega) = h_0 + V_H + \Sigma^{GW}(\omega)$ [117]. QS*GW* is thus a self-consistent perturbation theory where self-consistency determines the best H_0 within the *GW*A. Here we see that this static and Hermitian approximation to Σ^{GW} was chosen to conserve the quality of the diagonal terms. Once self-consistency is achieved, the eigenvalues of H_0 coincide with the (real part of the) poles of *GW* Green's function. In fact, at self-consistency the diagonal terms of the self-energy are precisely evaluated at the self-consistent quasiparticle energy E_i:

$$\left\langle \psi_i \middle| \Sigma^{\mathrm{QS}GW} \middle| \psi_i \right\rangle = \frac{1}{2}\left\{ \left\langle \psi_i \middle| \Sigma^{GW}(E_i) \middle| \psi_i \right\rangle + \left\langle \psi_i \middle| \Sigma^{GW}(E_i) \middle| \psi_i \right\rangle^* \right\} \tag{30}$$

and the only approximation for these terms is the neglect of the imaginary parts. Then the calculated quasiparticle band structures should be very similar to the *GW* ones.

4.3 Practical Implementation of the QSGW Method

The extension of an existing G_0W_0 code into a fully working QSGW code is straightforward. Instead of only calculating the diagonal matrix elements

$$\langle \psi_i | \Sigma^{GW} | \psi_i \rangle, \tag{31}$$

the implementation should also allow for $i \neq j$,

$$\langle \psi_i | \Sigma^{GW} | \psi_j \rangle. \tag{32}$$

Then compared to a simple G_0W_0 calculation, there is one additional convergence parameter: the extension of the range of states j. Indeed, after diagonalization of the QSGW Hamiltonian, the quasiparticle wavefunctions are expanded as a linear combination of Kohn–Sham orbitals:

$$|\Psi_i\rangle = \sum_j c_{ji} |\phi_j\rangle. \tag{33}$$

The c_{ji} coefficients form a unitary matrix, since both the quasiparticle wavefunctions and the Kohn–Sham wavefunctions form an orthonormal set. The accuracy of the expansion is of course governed by the flexibility of the basis set, i.e., the number of Kohn–Sham orbitals included in the right-hand side of (33). Fortunately, in all practical cases, the number of elements in the linear combination need not be as large as the original basis set.

Concerning computational time, there are two differences between QSGW and G_0W_0. Within QSGW, the GW self-energy has to be evaluated for all states used as a basis set in (33). For solids, this further implies the need to calculate the self-energy for all the $\mathbf{k}$-points in the grid. However in practice, the calculation of the self-energy is often not the limiting step of a QSGW run. This is rather the evaluation of the dielectric matrix used to construct W. This step is exactly the same for G_0W_0 and for QSGW. If this operation dominates the computer time consumption, the QSGW would be slower that G_0W_0 simply by the need to iterate the calculation of the dielectric matrix (typically 3–10 cycles). As a conclusion, the QSGW methods is roughly one order of magnitude slower than the usual G_0W_0 approximation for the most common cases.

4.4 Results

As mentioned earlier in this chapter, the G_0W_0 approach may experience problems when the starting point is inadequate. This is particularly true for crystals with very small or very large band gaps. In the first systematic study of QSGW for crystalline

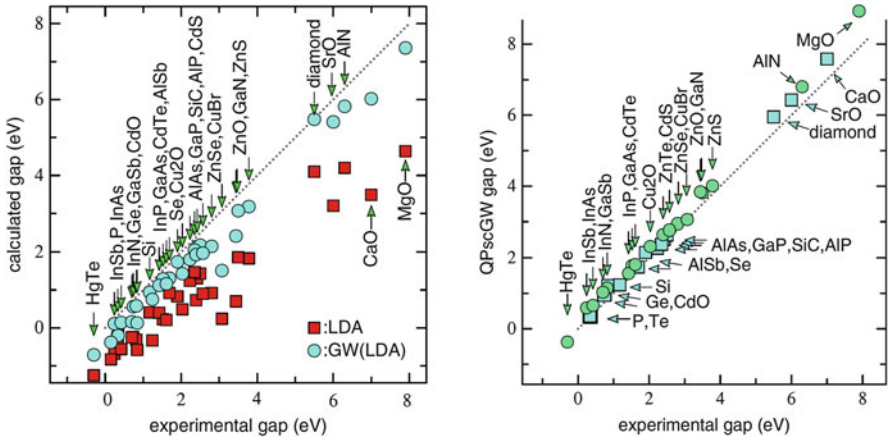

Fig. 7 Calculated band gaps compared to experimental band gaps within LDA and G_0W_0 (*left panel*), or within QS*GW* (*right panel*). $\Gamma - \Gamma$ direct gaps are shown as *circles* and other gaps as *squares*. The perfect agreement would be with all the points along the diagonal. Adapted from [117]. Copyright 2006, The American Physical Society

systems, van Schilfgaarde et al. [117] demonstrated the deficiencies of G_0W_0 (left panel of Fig. 7). The G_0W_0 band gaps generally slightly underestimate the experimental data.

The QS*GW* method then brings a clear improvement, as can be appreciated in the right panel of Fig. 7. For the small band-gap semiconductors, for which LDA wrongly predicted a metallic band structure, the improvement is spectacular. Whereas the G_0W_0 results were still affected by the wrong metallic starting point, the QS*GW* band gaps of InAs, InSb, and GaSb are quantitatively correct. For the large band-gap insulators, the LDA underestimation of the band gap is so dramatic that once again the G_0W_0 gaps are strongly affected by the starting point. The QS*GW* band gaps of diamond, MgO, CaO, etc., are closer to the experimental values.

The QS*GW* has been found to be particularly important for transition metal oxides such as MnO and NiO [71]. In particular, the elements with a complete *d* shell experience an unexpectedly large error in G_0W_0, as shown in Fig. 7 for ZnO and Cu_2O. For Cu_2O it was also shown that QS*GW* greatly improves both the photoemission spectroscopy and the optical spectrum [133], as obtained from the solution of the Bethe–Salpeter equation [14].

In order to judge the performance of an electronic-structure method, one should always consider more properties than just the band gaps. Indeed, QS*GW* generally improves with respect to LDA, as for effective masses and gaps at other critical points [118]. The bandwidth of Na is narrower in QS*GW* than in LDA, in agreement with experiment and with G_0W_0 (self-consistent *GW* results on the homogeneous electron gas, which is a very good approximation to sodium, instead had shown an increase of the bandwidth [67, 130]). In 3*d* metals (e.g., Ti, Cr, Fe, Co, Ni), the 3*d*

bandwidths, the exchange splittings, and magnetic moments are generally improved with respect to LDA [117], with some exceptions like Ni and other systems where LDA already overestimates the magnetic moment, and one expects that the coupling with spin fluctuations beyond *GW* should be taken into account [57]. In addition to spectroscopic data, some ground-state properties can also be successfully predicted with QS*GW*, such as electric field gradients [134]. Finally, QS*GW* results have also been used as a starting point for other calculations, like impact ionization rates [135] and the transverse spin susceptibility [136], again finding good agreement with experiment.

There is still an overall slight overestimation of the band gaps by the QS*GW* method, which is systematic in all compounds studied [117, 118]. The accuracy of QS*GW* somewhat deteriorates in *d* and *f* compounds with respect to *sp* systems. The unoccupied states are generally too high: by 0.2 eV for *sp* semiconductors, less than 1 eV for d^0 compounds like $SrTiO_3$ and TiO_2, more than 1 eV for other *d* materials like NiO, and up to 3 eV for *f* compounds like Gd and Er [119]. Most often these errors have been ascribed to the missing electron–hole interactions (excitonic effects) in the calculation of the polarization $\widetilde{\chi}$ and the screened interaction *W*, which is done at the RPA level in the *GW* approximation. The dielectric constants turn out to be too small (by ~20%) [117], resulting in a slight underscreening and, in turn, into too large gaps. Indeed, van Schilfgaarde and coworkers empirically found that by rescaling by 0.8 the screened interaction *W*, the results were improved (see, e.g., [123, 124, 137]). This tendency was later confirmed by Shishkin et al. [138], who corrected the remaining error with the inclusion of electron-hole interaction in *W* using the Nanoquanta kernel of time-dependent density-functional theory [139]. These observations mean that vertex corrections in Σ – see (13f)] – would play a secondary role in a large variety of materials. However, for example, the localized *d* band in the occupied valence band of materials like GaAs, GaN, and GaP, which is slightly too shallow, cannot be corrected by this simple rescaling that corrects the QS*GW* underscreening. A more detailed investigation of the effects of vertex corrections beyond *GW* is thus still an open issue.

Of course, not all the features of the full *GW* self-energy can be retained in QS*GW*. The simplicity has a price. Being a quasiparticle-only theory, all the properties beyond quasiparticles are naturally absent in QS*GW*. For instance, the satellites in the photoemission spectra of correlated [57] and non-correlated [56] materials are no longer accessible. The finite lifetimes of quasiparticles [58] are also beyond QS*GW*. A way to overcome this limitation is to use the QS*GW* results at self-consistency as a starting point to calculate the Green's function in the *GW* approximation and hence the spectral function, as has been done recently for $SrVO_3$ [107].

The QS*GW* has mostly been applied to solids. Nowadays, the first applications to atoms and molecules are being carried out by several groups. Bruneval [34] first applied QS*GW* to the ionization potential of small sodium clusters. Then Ke [140] demonstrated the improvement of QS*GW* compared to G_0W_0 based on Hartree–Fock for the conjugated molecules (C_nH_m) for electron affinities and ionization

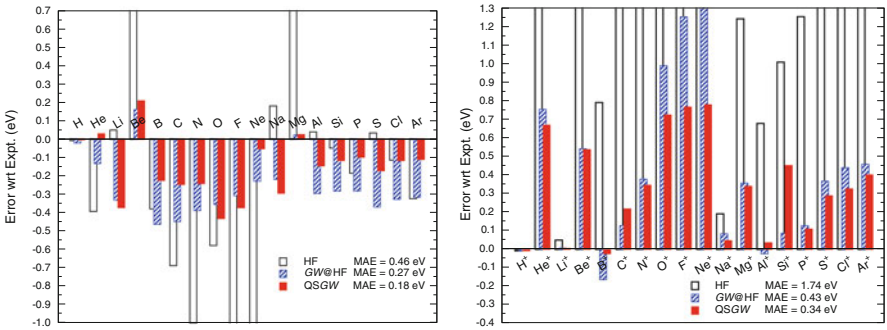

Fig. 8 Deviation from the experimental ionization potential of atoms as obtained from the HOMO of the neutral atoms (*left panel*) or from the LUMO of the positive ions (*right panel*), i.e., $\epsilon_{\mathrm{HOMO/LUMO}} - (-I)$. HF is presented with *open bars*, G_0W_0 based on HF inputs (*GW*@HF) with *striped bars*, and QS*GW* with *filled bars*. The mean absolute error (MAE) is also provided. Reprinted with permission from [141]. Copyright 2012, American Institute of Physics

potentials. More recently, Bruneval [141] investigated its performance for all the light atoms from H to Ar. As shown in Fig. 8, the improvement offered by QS*GW* is not systematic. On average QS*GW* performs better than G_0W_0 based on HF with a relatively smaller mean absolute error, although for specific atoms the opposite can hold true. Note that the error in the LUMO of the positive ion (right panel) remains rather large even for QS*GW*. Of course, the application of QS*GW* to molecules is still in its early stage and its performance has to be evaluated for a wider range of molecules, especially for large molecules.

5 Relation with Alternative Self-Consistent Schemes

Although the QS*GW* method is a simplified version of the full self-consistent *GW* self-energy, the calculations may still be quite cumbersome. Many authors resort to even more approximated types of self-consistency. This section briefly describes the alternatives to QS*GW*.

5.1 Energy-Only Self-Consistency

In the energy-only self-consistent *GW* scheme, the eigenvalues used to build G and W are updated iteratively, while the wavefunctions are kept at the level of the mean-field starting point. This scheme corresponds to keeping only the diagonal terms of the QS*GW* Hamiltonian. Thus whenever the mean-field orbitals are a good approximation to QP wavefunctions, the two schemes will give very similar results. Of

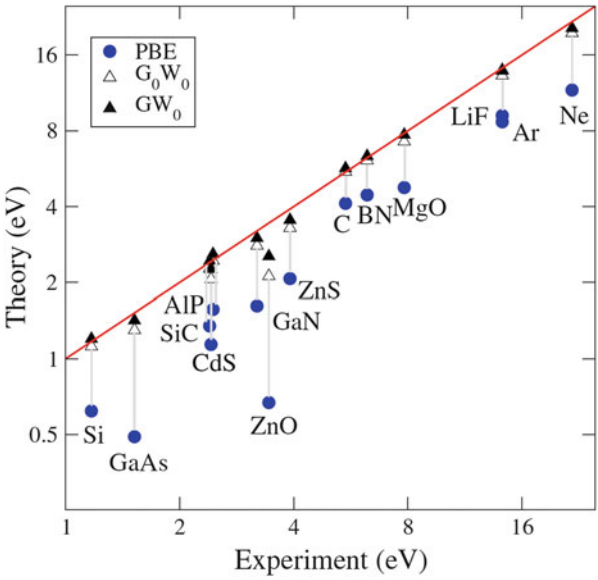

Fig. 9 Comparison of band gaps calculated in GGA (PBE), G_0W_0, and GW_0, with experiment for a series of prototypical *sp* semiconductors and insulators. GW_0 performs best. From [145]. Copyright 2007, The American Physical Society

course, the energy-only self-consistent *GW* is computationally much cheaper than QS*GW*.

This scheme has been used many times in the past [83, 142–145] in order to improve band gaps and band widths with respect to G_0W_0 results. Recently, Shishkin and Kresse [145] presented a systematic study of the band gap of several *sp* semiconductors and insulators. The conclusion of their analysis is that updating the eigenvalues in G while keeping W at the GGA level (the scheme is called GW_0) gives the best results in comparison to experiment (see Fig. 9). This is due to a cancellation of effects between the band-gap opening and excitonic interactions in W that is verified in the class of materials considered in [145]. In turn, the GGA screening is in better agreement with the physical one (i.e., the one that can be measured by loss spectroscopies) than the screening calculated self-consistently. In fact, updating the eigenvalues in W also leads to an underscreening and further opens the gaps, causing the results to deteriorate [145]. Similar conclusions can be reached in finite systems. For instance, Blase and coworkers [94, 146] recently found that in a set of organic molecules and DNA/RNA nucleobases the energy-only self-consistent *GW* scheme provides much better results than G_0W_0 on top of LDA.

5.2 *Alternatives to the QSGW: COHSEX and Others*

COHSEX is a static and Hermitian approximation to the *GW* self-energy (see Sect. 2.4). In this respect it parallels the self-energy of the QS*GW* approximation.

The difference between the two approximations is the fact that in COHSEX the screening is static (i.e., it is calculated only at $\omega = 0$), while it is fully dynamical in QS*GW*.

Bruneval, Vast, and Reining [112] proposed to combine self-consistent COHSEX with a subsequent G_0W_0 calculation, giving very similar results to QS*GW* [112, 133] at a much lower computational cost. In fact, in COHSEX both the calculations of the screening (only static) and the self-energy (depending only on occupied states) are cheaper than in *GW*. COHSEX alone generally overestimates band gaps and dynamical effects contained in the *GW* self-energy are needed to correct this overestimation. In many cases a perturbative G_0W_0 correction is sufficient, while, for example, in prototypical transition metal oxides like NiO and MnO, a self-consistent update of the eigenvalues is needed to get results similar to QS*GW* [147, Gatti and Rubio (2013) Unpublished].

The COHSEX+ G_0W_0 scheme has been successfully applied in a wide range of materials: from transition metal compounds (e.g., Cu_2O, VO_2, $NiS_{2-x}Se_x$ [105, 126, 133]) to CIGS and quaternary chalcogenides [120, 125, 148], delafossite transparent conductive oxides [121, 149], and intermediate-band materials [150, 151].

In an earlier work, Gygi and Baldereschi derived a simplified model static self-energy from the *GW* approximation [152] that was later used in a self-consistent manner in several transition metal oxides (e.g., MnO, NiO, $CaCuO_2$, and VO_2 [153–155]). These applications employed a model screened interaction W in which the static dielectric constant was a parameter taken from experiment. Nevertheless, together with the work of Aryasetiawan and Gunnarsson on NiO [156], in which the self-consistency was simulated by adding to LDA a static correction term for the Ni e_g bands, they provided the first meaningful *GW* descriptions of these transition metal oxides beyond the G_0W_0 scheme.

More recently, Sakuma, Miyake, and Aryasetiawan have proposed an alternative self-consistent quasiparticle scheme that is based on Löwdin's method of symmetric orthogonalization [157]. Results have been found to be very close to those in the QS*GW* scheme.

5.3 Hybrid Functionals and LDA+U

Hybrid functionals [158] and the LDA+U approach [159] have become very popular as improved exchange-correlation DFT functionals in solids. At the same time, both can be seen as an approximation to the *GW* self-energy [160, 161]. In hybrids like the Heyd–Scuseria–Ernzerhof (HSE) functional [158] the α and ω parameters, which are obtained by considerations of the adiabatic-connection formula and numerically fitting the results against a benchmark set of data, play the role of effective screening. In LDA+U the on-site Hubbard U correction is only applied to a subset of states (and a double-counting correction is introduced). The electron–electron local interaction is treated at the Hartree–Fock level and the screening of the interaction is effectively obtained by reducing U from its atomic

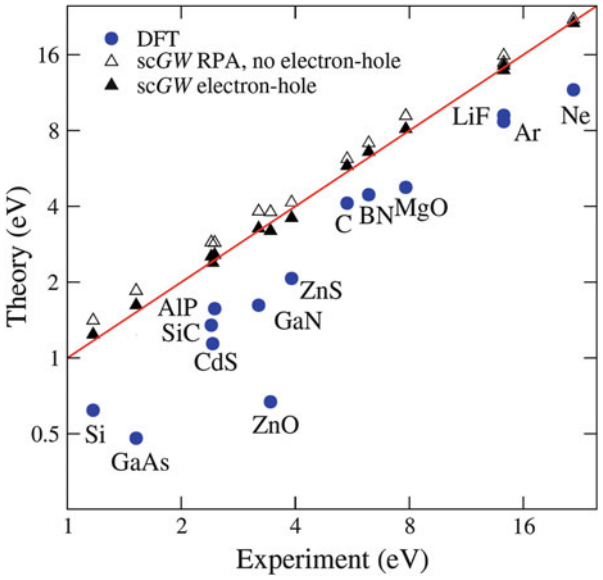

Fig. 10 Comparison of band gaps calculated in GGA (PBE), HSE and G_0W_0 on top of them with experiment for a series of prototypical *sp* semiconductors and insulators. HSE is a better starting point than GGA. From [102]. Copyright © 2009 WILEY-VCH Verlag GmbH & Co. KGaA, Weinheim

values. The Hubbard U can be pragmatically used as fitting parameter or calculated for example in RPA: in this case all the electrons not belonging to the chosen subset of states are then providing the effective screening of U [162]. The common effect of both hybrid functionals and LDA+U is to produce, as a result of an exchange effect, a localization of the LDA orbitals that for d and f electrons are generally too delocalized.

Even though both methods depend on parameters, they can be seen as a cheap way to perform self-consistent quasiparticle calculations. In fact, in recent years they have been proposed as an improved starting point for subsequent G_0W_0 calculations. In particular, Rödl and coworkers [163–165] have shown that in prototypical transition metal oxides it is possible to fit the more expensive HSE results from GGA+U calculations with an additional scissor shift, producing results in good agreement with experiments. The application of these computationally efficient schemes is also gaining quite a large popularity in the *GW* community (see, e.g., [99–101, 122, 163–173] and [102] for an early review; Fig. 10 contains a collection of results from the latter).

Besides the presence of parameters, the most important drawback with respect to QS*GW* is their limited transferability, which is restricted by the limited flexibility of their description of the screening of the Coulomb interaction (which in *GW* is explicitly accounted for). This can become an important issue in situations where the screening is substantially changing as a function of an external control parameter: for example, in the study of metal-insulator transitions under pressure [Gatti and Rubio (2013) Unpublished] and for materials characterized by a strong interplay between structure and electronic properties such as the CIGS [120]. In these cases QS*GW* is expected to be better (also with respect to G_0W_0).

6 Conclusions and Outlook

The present chapter aimed at presenting the robustness and the simplicity of the QS*GW* when addressing the spectral properties of materials. The QS*GW* method is nowadays a mature theory that offers a remarkable trade-off between speed and accuracy.

It has been applied to an impressively wide variety of materials, covering the range from sodium [113] to uranium and plutonium [174, 175], and including metals, semi-conductors, insulators, atoms, and molecules. The comparison to experiment is in general very favorable. Therefore, in our opinion, QS*GW* is, to date, the best ab initio method available to calculate the quasiparticle spectrum of photoemission (and inverse photoemission) for solid state systems and can be thought of as a predictive theory.

Furthermore, QS*GW* is readily available in popular codes, such as Abinit [176] or Vasp [177]. On the other hand, the increasing popularity of the method nowadays goes hand in hand with the need for optimizing the computational algorithms, in order to prevent slow convergence in the self-consistency (see, e.g., [178]).

The QS*GW* method has enlarged the range of compounds that can be described by the *GW* approximation. It has demonstrated that, for materials for which G_0W_0 was performing badly and thus considered out of reach for ab initio methods (e.g. "strongly correlated" transition metal oxides), the failure was to be ascribed to the perturbative scheme of G_0W_0, and not to the *GW* approximation itself [71].

QS*GW* has provided an accurate reference from which it now makes sense to investigate more refined features of the electronic structure of materials, such as electron–phonon coupling [61, 62] and lattice polarization [179], which now are larger than the error bar of the method. Analogously, the field is now ready to study effects of electron interaction beyond the *GW* approximation (i.e., vertex corrections, for example, through the coupling with other approximations), without the bias that the perturbative G_0W_0 scheme introduces.

Acknowledgments We thank Mark van Schilfgaarde for a critical reading of the chapter.

References

1. Hüfner S (2010) Photoelectron spectroscopy, 3rd edn. Springer, Berlin
2. Damascelli A, Hussain Z, Shen ZX (2003) Rev Mod Phys 75:473. doi:10.1103/RevModPhys.75.473
3. Bardyszewski W, Hedin L (1985) Phys Scripta 32(4):439
4. Hedin L, Michiels J, Inglesfield J (1998) Phys Rev B 58:15565. doi:10.1103/PhysRevB.58.15565
5. Hedin L (1999) J Phys Condens Matter 11(42):R489
6. Braun J (1996) Rep Prog Phys 59(10):1267
7. Minár J, Braun J, Mankovsky S, Ebert H (2011) advances in vacuum ultraviolet and X-ray physics: the 37th international conference on vacuum ultraviolet and X-ray physics

(VUVX2010). J Electron Spectros Relat Phenomena 184(36):91. doi:10.1016/j.elspec.2011.01.009
8. Minár J, Braun J, Ebert H (2012) J Electron Spectrosc Relat Phenomena (0). doi:10.1016/j.elspec.2012.10.003
9. Papalazarou E, Gatti M, Marsi M, Brouet V, Iori F, Reining L, Annese E, Vobornik I, Offi F, Fondacaro A, Huotari S, Lacovig P, Tjernberg O, Brookes NB, Sacchi M, Metcalf P, Panaccione G (2009) Phys Rev B 80:155115. doi:10.1103/PhysRevB.80.155115
10. Hohenberg P, Kohn W (1964) Phys Rev 136(3B):B864. doi:10.1103/PhysRev.136.B864
11. Kohn W, Sham LJ (1965) Phys Rev 140:A1133. doi:10.1103/PhysRev.140.A1133
12. Sham LJ, Kohn W (1966) Phys Rev 145:561. doi:10.1103/PhysRev.145.561
13. Janak JF (1978) Phys Rev B 18:7165. doi:10.1103/PhysRevB.18.7165
14. Onida G, Reining L, Rubio A (2002) Rev Mod Phys 74:601. doi:10.1103/RevModPhys.74.601
15. Godby RW, White ID (1998) Phys Rev Lett 80:3161. doi:10.1103/PhysRevLett.80.3161
16. Sham LJ, Schlüter M (1983) Phys Rev Lett 51:1888. doi:10.1103/PhysRevLett.51.1888
17. Perdew JP, Levy M (1983) Phys Rev Lett 51:1884. doi:10.1103/PhysRevLett.51.1884
18. Godby RW, Schlüter M, Sham LJ (1986) Phys Rev Lett 56:2415. doi:10.1103/PhysRevLett.56.2415
19. Holzmann M, Bernu B, Pierleoni C, McMinis J, Ceperley DM, Olevano V, Delle Site L (2011) Phys Rev Lett 107:110402. doi:10.1103/PhysRevLett.107.110402
20. Gatti M, Olevano V, Reining L, Tokatly IV (2007) Phys Rev Lett 99:057401. doi:10.1103/PhysRevLett.99.057401
21. Booth GH, Gruneis A, Kresse G, Alavi A (2013) Nature 493(7432):365
22. Fetter AL, Walecka JD (1971) Quantum theory of many-particle systems. MacGraw-Hill, New York
23. Mahan GD (1981) Many-particle physics. Plenum, New York
24. Gross EKU, Runge E, Heinonen O (1991) Many-particle theory. Adam Hilger, Bristol
25. Hedin L (1965) Phys Rev 139:A796. doi:10.1103/PhysRev.139.A796
26. Hedin L, Lundqvist S (1970) Academic, pp 1–181. doi:10.1016/S0081-1947(08)60615-3
27. Aryasetiawan F, Gunnarsson O (1998) Rep Prog Phys 61(3):237
28. Aulbur WG, Jönsson L, Wilkins JW (1999) Academic, pp 1–218. doi:10.1016/S0081-1947(08)60248-9
29. Shaltaf R, Rignanese GM, Gonze X, Giustino F, Pasquarello A (2008) Phys Rev Lett 100:186401. doi:10.1103/PhysRevLett.100.186401
30. Wang NP, Rohlfing M, Krüger P, Pollmann J (2005) Phys Rev B 71:045407. doi:10.1103/PhysRevB.71.045407
31. Thygesen KS, Rubio A (2009) Phys Rev Lett 102:046802. doi:10.1103/PhysRevLett.102.046802
32. Garcia-Lastra JM, Rostgaard C, Rubio A, Thygesen KS (2009) Phys Rev B 80:245427. doi:10.1103/PhysRevB.80.245427
33. Rinke P, Janotti A, Scheffler M, Van de Walle CG (2009) Phys Rev Lett 102:026402. doi:10.1103/PhysRevLett.102.026402
34. Bruneval F (2009) Phys Rev Lett 103:176403. doi:10.1103/PhysRevLett.103.176403
35. Bockstedte M, Marini A, Pankratov O, Rubio A (2010) Phys Rev Lett 105:026401. doi:10.1103/PhysRevLett.105.026401
36. Ma Y, Rohlfing M, Gali A (2010) Phys Rev B 81:041204. doi:10.1103/PhysRevB.81.041204
37. Jain M, Chelikowsky JR, Louie SG (2011) Phys Rev Lett 107:216803. doi:10.1103/PhysRevLett.107.216803
38. Bruneval F, Roma G (2011) Phys Rev B 83:144116. doi:10.1103/PhysRevB.83.144116
39. Neaton JB, Hybertsen MS, Louie SG (2006) Phys Rev Lett 97:216405. doi:10.1103/PhysRevLett.97.216405
40. Darancet P, Ferretti A, Mayou D, Olevano V (2007) Phys Rev B 75:075102. doi:10.1103/PhysRevB.75.075102

41. Thygesen KS, Rubio A (2008) Phys Rev B 77:115333. doi:10.1103/PhysRevB.77.115333
42. Myöhänen P, Stan A, Stefanucci G, van Leeuwen R (2009) Phys Rev B 80:115107. doi:10.1103/PhysRevB.80.115107
43. Rangel T, Ferretti A, Trevisanutto PE, Olevano V, Rignanese GM (2011) Phys Rev B 84:045426. doi:10.1103/PhysRevB.84.045426
44. Reining L, Onida G, Godby RW (1997) Phys Rev B 56:R4301. doi:10.1103/PhysRevB.56.R4301
45. Bruneval F, Gonze X (2008) Phys Rev B 78:085125. doi:10.1103/PhysRevB.78.085125
46. Umari P, Stenuit G, Baroni S (2010) Phys Rev B 81:115104. doi:10.1103/PhysRevB.81.115104
47. Giustino F, Cohen ML, Louie SG (2010) Phys Rev B 81:115105. doi:10.1103/PhysRevB.81.115105
48. Berger JA, Reining L, Sottile F (2010) Phys Rev B 82:041103. doi:10.1103/PhysRevB.82.041103
49. Nguyen HV, Pham TA, Rocca D, Galli G (2012) Phys Rev B 85:081101. doi:10.1103/PhysRevB.85.081101
50. Bruneval F, Sottile F, Olevano V, Del Sole R, Reining L (2005) Phys Rev Lett 94:186402. doi:10.1103/PhysRevLett.94.186402. URL
51. Nelson W, Bokes P, Rinke P, Godby RW (2007) Phys Rev A 75:032505. doi:10.1103/PhysRevA.75.032505
52. Morris AJ, Stankovski M, Delaney KT, Rinke P, García-González P, Godby RW (2007) Phys Rev B 76:155106. doi:10.1103/PhysRevB.76.155106
53. Romaniello P, Guyot S, Reining L (2009) J Chem Phys 131(15):154111. doi:10.1063/1.3249965
54. Caruso F, Rohr DR, Hellgren M, Ren X, Rinke P, Rubio A, Scheffler M (2013) Phys Rev Lett 110:146403. doi:10.1103/PhysRevLett.110.146403
55. Aryasetiawan F, Hedin L, Karlsson K (1996) Phys Rev Lett 77:2268. doi:10.1103/PhysRevLett.77.2268
56. Guzzo M, Lani G, Sottile F, Romaniello P, Gatti M, Kas JJ, Rehr JJ, Silly MG, Sirotti F, Reining L (2011) Phys Rev Lett 107:166401. doi:10.1103/PhysRevLett.107.166401
57. Springer M, Aryasetiawan F, Karlsson K (1998) Phys Rev Lett 80:2389. doi:10.1103/PhysRevLett.80.2389
58. Zhukov VP, Chulkov EV, Echenique PM (2004) Phys Rev Lett 93:096401. doi:10.1103/PhysRevLett.93.096401
59. Romaniello P, Bechstedt F, Reining L (2012) Phys Rev B 85:155131. doi:10.1103/PhysRevB.85.155131
60. Biermann S, Aryasetiawan F, Georges A (2003) Phys Rev Lett 90:086402. doi:10.1103/PhysRevLett.90.086402
61. Giustino F, Louie SG, Cohen ML (2010) Phys Rev Lett 105:265501. doi:10.1103/PhysRevLett.105.265501
62. Cannuccia E, Marini A (2011) Phys Rev Lett 107:255501. doi:10.1103/PhysRevLett.107.255501
63. Dahlen NE, van Leeuwen R (2007) Phys Rev Lett 98:153004. doi:10.1103/PhysRevLett.98.153004
64. von Friesen MP, Verdozzi C, Almbladh CO (2009) Phys Rev Lett 103:176404. doi:10.1103/PhysRevLett.103.176404
65. Puig von Friesen M, Verdozzi C, Almbladh CO (2010) Phys Rev B 82:155108. doi:10.1103/PhysRevB.82.155108
66. Schindlmayr A, Pollehn TJ, Godby RW (1998) Phys Rev B 58:12684. doi:10.1103/PhysRevB.58.12684
67. Holm B, von Barth U (1998) Phys Rev B 57:2108. doi:10.1103/PhysRevB.57.2108
68. Holm B (1999) Phys Rev Lett 83:788. doi:10.1103/PhysRevLett.83.788

69. García-González P, Godby RW (2001) Phys Rev B 63:075112. doi:10.1103/PhysRevB.63.075112
70. Ismail-Beigi S (2010) Phys Rev B 81:195126. doi:10.1103/PhysRevB.81.195126
71. Faleev SV, van Schilfgaarde M, Kotani T (2004) Phys Rev Lett 93:126406. doi:10.1103/PhysRevLett.93.126406
72. Strinati G (1988) Rivista del Nuovo Cimento 11:1
73. Møller C, Plesset MS (1934) Phys Rev 46:618. doi:10.1103/PhysRev.46.618
74. Adler SL (1963) Phys Rev 130:1654. doi:10.1103/PhysRev.130.1654
75. Wiser N (1963) Phys Rev 129:62. doi:10.1103/PhysRev.129.62
76. Strinati G, Mattausch HJ, Hanke W (1980) Phys Rev Lett 45:290. doi:10.1103/PhysRevLett.45.290
77. Hybertsen MS, Louie SG (1985) Phys Rev Lett 55:1418. doi:10.1103/PhysRevLett.55.1418
78. Shirley EL, Martin RM (1993) Phys Rev B 47:15404. doi:10.1103/PhysRevB.47.15404
79. Hedin L, Lundqvist B, Lundqvist S (1967) Solid State Commun 5(4):237. doi:10.1016/0038-1098(67)90264-5
80. Lundqvist B (1967) Physik der kondensierten Materie 6(3):193. doi:10.1007/BF02422716
81. Blomberg C, Bergersen B (1972) Can J Phys 50(19):2286. doi:10.1139/p72-303
82. Bergersen B, Kus FW, Blomberg C (1973) Can J Phys 51(1):102. doi:10.1139/p73-012
83. Hybertsen MS, Louie SG (1986) Phys Rev B 34:5390. doi:10.1103/PhysRevB.34.5390
84. Godby RW, Needs RJ (1989) Phys Rev Lett 62(10):1169. doi:10.1103/PhysRevLett.62.1169
85. Lebègue S, Arnaud B, Alouani M, Bloechl PE (2003) Phys Rev B 67(15):155208. doi:10.1103/PhysRevB.67.155208
86. Morin FJ (1959) Phys Rev Lett 3(1):34. doi:10.1103/PhysRevLett.3.34
87. Del Sole R, Reining L, Godby RW (1994) Phys Rev B 49:8024. doi:10.1103/PhysRevB.49.8024
88. Cazzaniga M (2012) Phys Rev B 86:035120. doi:10.1103/PhysRevB.86.035120
89. Marini A, Rubio A (2004) Phys Rev B 70:081103. doi:10.1103/PhysRevB.70.081103
90. Stankovski M (2008) Local and non-local vertex corrections beyond the GW approximation. Ph.D. thesis, University of York
91. Rostgaard C, Jacobsen KW, Thygesen KS (2010) Phys Rev B 81:085103. doi:10.1103/PhysRevB.81.085103
92. Bruneval F, Marques MAL (2013) J Chem Theory Comput 9(1):324. doi:10.1021/ct300835h
93. Stan A, Dahlen NE, van Leeuwen R (2006) Europhys Lett 76(2):298
94. Blase X, Attaccalite C, Olevano V (2011) Phys Rev B 83:115103. doi:10.1103/PhysRevB.83.115103
95. Caruso F, Rinke P, Ren X, Scheffler M, Rubio A (2012) Phys Rev B 86:081102. doi:10.1103/PhysRevB.86.081102
96. Marom N, Caruso F, Ren X, Hofmann OT, Körzdörfer T, Chelikowsky JR, Rubio A, Scheffler M, Rinke P (2012) Phys Rev B 86:245127. doi:10.1103/PhysRevB.86.245127
97. Rinke P, Qteish A, Neugebauer J, Freysoldt C, Scheffler M (2005) New J Phys 7(1):126
98. Rinke P, Qteish A, Neugebauer J, Scheffler M (2008) Phys Status Solidi B 245(5):929. doi:10.1002/pssb.200743380
99. Miyake T, Zhang P, Cohen ML, Louie SG (2006) Phys Rev B 74:245213. doi:10.1103/PhysRevB.74.245213
100. Jiang H, Gomez-Abal RI, Rinke P, Scheffler M (2009) Phys Rev Lett 102:126403. doi:10.1103/PhysRevLett.102.126403
101. Fuchs F, Furthmüller J, Bechstedt F, Shishkin M, Kresse G (2007) Phys Rev B 76:115109. doi:10.1103/PhysRevB.76.115109
102. Bechstedt F, Fuchs F, Kresse G (2009) Phys Status Solidi B 246(8):1877. doi:10.1002/pssb.200945074
103. Koethe TC, Hu Z, Haverkort MW, Schüßler-Langeheine C, Venturini F, Brookes NB, Tjernberg O, Reichelt W, Hsieh HH, Lin HJ, Chen CT, Tjeng LH (2006) Phys Rev Lett 97:116402. doi:10.1103/PhysRevLett.97.116402

104. Sakuma R, Miyake T, Aryasetiawan F (2008) Phys Rev B 78:075106. doi:10.1103/PhysRevB.78.075106
105. Gatti M, Bruneval F, Olevano V, Reining L (2007) Phys Rev Lett 99:266402. doi:10.1103/PhysRevLett.99.266402
106. Pollehn TJ, Schindlmayr A, Godby RW (1998) J Phys Condens Matter 10(6):1273
107. Gatti M, Guzzo M (2013) Phys Rev B 87:155147. doi:10.1103/PhysRevB.87.155147
108. Rohlfing M, Louie SG (2000) Phys Rev B 62:4927. doi:10.1103/PhysRevB.62.4927
109. White ID, Godby RW, Rieger MM, Needs RJ (1998) Phys Rev Lett 80:4265. doi:10.1103/PhysRevLett.80.4265
110. Pulci O, Bechstedt F, Onida G, Del Sole R, Reining L (1999) Phys Rev B 60:16758. doi:10.1103/PhysRevB.60.16758
111. Rohlfing M, Wang NP, Krüger P, Pollmann J (2003) Phys Rev Lett 91:256802. doi:10.1103/PhysRevLett.91.256802
112. Bruneval F, Vast N, Reining L (2006) Phys Rev B 74:045102. doi:10.1103/PhysRevB.74.045102
113. van Schilfgaarde M, Kotani T, Faleev SV (2006) Phys Rev B 74:245125. doi:10.1103/PhysRevB.74.245125
114. Marsili M, Pulci O, Bechstedt F, Del Sole R (2005) Phys Rev B 72:115415. doi:10.1103/PhysRevB.72.115415
115. Wentzcovitch RM, Schulz WW, Allen PB (1994) Phys Rev Lett 72:3389. doi:10.1103/PhysRevLett.72.3389
116. Zylbersztejn A, Mott NF (1975) Phys Rev B 11:4383. doi:10.1103/PhysRevB.11.4383
117. van Schilfgaarde M, Kotani T, Faleev S (2006) Phys Rev Lett 96:226402. doi:10.1103/PhysRevLett.96.226402
118. Kotani T, van Schilfgaarde M, Faleev SV (2007) Phys Rev B 76:165106. doi:10.1103/PhysRevB.76.165106
119. Chantis AN, van Schilfgaarde M, Kotani T (2007) Phys Rev B 76:165126. doi:10.1103/PhysRevB.76.165126
120. Vidal J, Botti S, Olsson P, Guillemoles JF, Reining L (2010) Phys Rev Lett 104:056401
121. Vidal J, Trani F, Bruneval F, Marques MAL, Botti S (2010) Phys Rev Lett 104:136401. doi:10.1103/PhysRevLett.104.136401
122. Franchini C, Sanna A, Marsman M, Kresse G (2010) Phys Rev B 81:085213. doi:10.1103/PhysRevB.81.085213
123. Svane A, Christensen NE, Cardona M, Chantis AN, van Schilfgaarde M, Kotani T (2010) Phys Rev B 81:245120. doi:10.1103/PhysRevB.81.245120
124. Svane A, Christensen NE, Cardona M, Chantis AN, van Schilfgaarde M, Kotani T (2011) Phys Rev B 84:205205. doi:10.1103/PhysRevB.84.205205
125. Aguilera I, Vidal J, Wahnón P, Reining L, Botti S (2011) Phys Rev B 84:085145. doi:10.1103/PhysRevB.84.085145
126. Schuster C, Gatti M, Rubio A (2012) Eur Phys J B 85:1. doi:10.1140/epjb/e2012-30384-7
127. Baroni S, Resta R (1986) Phys Rev B 33(10):7017. doi:10.1103/PhysRevB.33.7017
128. Baym G, Kadanoff LP (1961) Phys Rev 124:287. doi:10.1103/PhysRev.124.287
129. Schindlmayr A, García-González P, Godby RW (2001) Phys Rev B 64:235106. doi:10.1103/PhysRevB.64.235106
130. Shirley EL (1996) Phys Rev B 54:7758. doi:10.1103/PhysRevB.54.7758
131. Bechstedt F, Tenelsen K, Adolph B, Del Sole R (1997) Phys Rev Lett 78:1528. doi:10.1103/PhysRevLett.78.1528
132. Stan A, Dahlen NE, van Leeuwen R (2009) J Chem Phys 130(11):114105. doi:10.1063/1.3089567
133. Bruneval F, Vast N, Reining L, Izquierdo M, Sirotti F, Barrett N (2006) Phys Rev Lett 97:267601. doi:10.1103/PhysRevLett.97.267601
134. Christensen NE, Svane A, Laskowski R, Palanivel B, Modak P, Chantis AN, van Schilfgaarde M, Kotani T (2010) Phys Rev B 81:045203. doi:10.1103/PhysRevB.81.045203

135. Kotani T, van Schilfgaarde M (2010) Phys Rev B 81:125201. doi:10.1103/PhysRevB.81.125201
136. Kotani T, van Schilfgaarde M (2008) J Phys Condens Matter 20(29):295214
137. Punya A, Lambrecht WRL, van Schilfgaarde M (2011) Phys Rev B 84:165204. doi:10.1103/PhysRevB.84.165204
138. Shishkin M, Marsman M, Kresse G (2007) Phys Rev Lett 99:246403. doi:10.1103/PhysRevLett.99.246403
139. Botti S, Schindlmayr A, Sole RD, Reining L (2007) Rep Prog Phys 70(3):357
140. Ke SH (2011) Phys Rev B 84:205415. doi:10.1103/PhysRevB.84.205415
141. Bruneval F (2012) J Chem Phys 136(19):194107. doi:10.1063/1.4718428
142. Northrup JE, Hybertsen MS, Louie SG (1987) Phys Rev Lett 59:819. doi:10.1103/PhysRevLett.59.819
143. Luo W, Ismail-Beigi S, Cohen ML, Louie SG (2002) Phys Rev B 66:195215. doi:10.1103/PhysRevB.66.195215
144. Fleszar A, Hanke W (2005) Phys Rev B 71:045207. doi:10.1103/PhysRevB.71.045207
145. Shishkin M, Kresse G (2007) Phys Rev B 75:235102. doi:10.1103/PhysRevB.75.235102
146. Faber C, Attaccalite C, Olevano V, Runge E, Blase X (2011) Phys Rev B 83:115123. doi:10.1103/PhysRevB.83.115123
147. Guzzo M (2008) Exchange and correlation effects in the electronic properties of transition metal oxides: the example of NiO. Master's thesis, Università degli studi di Milano-Bicocca
148. Botti S, Kammerlander D, Marques MAL (2011) Appl Phys Lett, 98(24). doi: 10.1063/1.3600060
149. Trani F, Vidal J, Botti S, Marques MAL (2010) Phys Rev B 82:085115. doi:10.1103/PhysRevB.82.085115
150. Aguilera I, Palacios P, Wahnón P (2011) Phys Rev B 84:115106. doi:10.1103/PhysRevB.84.115106
151. Lucero MJ, Aguilera I, Diaconu CV, Palacios P, Wahnón P, Scuseria GE (2011) Phys Rev B 83:205128. doi:10.1103/PhysRevB.83.205128
152. Gygi F, Baldereschi A (1989) Phys Rev Lett 62:2160. doi:10.1103/PhysRevLett.62.2160
153. Massidda S, Continenza A, Posternak M, Baldereschi A (1995) Phys Rev Lett 74:2323. doi:10.1103/PhysRevLett.74.2323
154. Massidda S, Continenza A, Posternak M, Baldereschi A (1997) Phys Rev B 55:13494. doi:10.1103/PhysRevB.55.13494
155. Continenza A, Massidda S, Posternak M (1999) Phys Rev B 60:15699. doi:10.1103/PhysRevB.60.15699
156. Aryasetiawan F, Gunnarsson O (1995) Phys Rev Lett 74:3221. doi:10.1103/PhysRevLett.74.3221
157. Sakuma R, Miyake T, Aryasetiawan F (2009) Phys Rev B 80:235128. doi:10.1103/PhysRevB.80.235128
158. Heyd J, Scuseria GE, Ernzerhof M (2006) J Chem Phys 124(21):219906. doi:10.1063/1.2204597
159. Anisimov VI, Zaanen J, Andersen OK (1991) Phys Rev B 44:943. doi:10.1103/PhysRevB.44.943
160. Anisimov VI, Aryasetiawan F, Lichtenstein AI (1997) J Phys Condens Matter 9(4):767
161. Marques MAL, Vidal J, Oliveira MJT, Reining L, Botti S (2011) Phys Rev B 83:035119. doi:10.1103/PhysRevB.83.035119
162. Aryasetiawan F, Karlsson K, Jepsen O, Schönberger U (2006) Phys Rev B 74:125106. doi:10.1103/PhysRevB.74.125106
163. Rödl C, Fuchs F, Furthmüller J, Bechstedt F (2008) Phys Rev B 77:184408. doi:10.1103/PhysRevB.77.184408
164. Rödl C, Fuchs F, Furthmüller J, Bechstedt F (2009) Phys Rev B 79:235114. doi:10.1103/PhysRevB.79.235114

165. Schleife A, Rödl C, Fuchs F, Furthmüller J, Bechstedt F (2009) Phys Rev B 80:035112. doi:10.1103/PhysRevB.80.035112
166. Kioupakis E, Zhang P, Cohen ML, Louie SG (2008) Phys Rev B 77:155114. doi:10.1103/PhysRevB.77.155114
167. Kobayashi S, Nohara Y, Yamamoto S, Fujiwara T (2008) Phys Rev B 78:155112. doi:10.1103/PhysRevB.78.155112
168. Jiang H, Gomez-Abal RI, Rinke P, Scheffler M (2010) Phys Rev B 82:045108. doi:10.1103/PhysRevB.82.045108
169. Jiang H, Rinke P, Scheffler M (2012) Phys Rev B 86:125115. doi:10.1103/PhysRevB.86.125115
170. Schleife A, Rödl C, Fuchs F, Furthmüller J, Bechstedt F (2007) Appl Phys Lett 91 (24):241915. doi:10.1063/1.2825277
171. Fuchs F, Bechstedt F (2008) Phys Rev B 77:155107. doi:10.1103/PhysRevB.77.155107
172. Schleife A, Varley JB, Fuchs F, Rödl C, Bechstedt F, Rinke P, Janotti A, Van de Walle CG (2011) Phys Rev B 83:035116. doi:10.1103/PhysRevB.83.035116
173. Riefer A, Fuchs F, Rödl C, Schleife A, Bechstedt F, Goldhahn R (2011) Phys Rev B 84:075218. doi:10.1103/PhysRevB.84.075218
174. Chantis AN, Albers RC, Jones MD, van Schilfgaarde M, Kotani T (2008) Phys Rev B 78:081101. doi:10.1103/PhysRevB.78.081101
175. Svane A, Albers RC, Christensen NE, van Schilfgaarde M, Chantis AN, Zhu JX (2013) Phys Rev B 87:045109. doi:10.1103/PhysRevB.87.045109
176. Gonze X, Amadon B, Anglade PM, Beuken JM, Bottin F, Boulanger P, Bruneval F, Caliste D, Caracas R, Cote M, Deutsch T, Genovese L, Ghosez P, Giantomassi M, Goedecker S, Hamann DR, Hermet P, Jollet F, Jomard G, Leroux S, Mancini M, Mazevet S, Oliveira MJT, Onida G, Pouillon Y, Rangel T, Rignanese GM, Sangalli D, Shaltaf R, Torrent M, Verstraete MJ, Zerah G, Zwanziger JW (2009) Comput Phys Commun 180:2582
177. Kresse G, Furthmüller J (1996) Comput Mater Sci 6(1):15. doi:10.1016/0927-0256(96)00008-0
178. Liao P, Carter EA (2011) Phys Chem Chem Phys 13:15189. doi:10.1039/C1CP20829B
179. Botti S, Marques MAL (2013) Phys Rev Lett 110:226404. doi:10.1103/PhysRevLett.110.226404